remote sensing

MDPI

Article

Influence of Precipitation Effects Induced by Large-Scale Irrigation in Northwest China on Soil Erosion in the Yellow River Basin

Ya Huang [1], Yong Zhao [2], Guiping Li [1], Jing Yang [1] and Yanping Li [1,*]

[1] College of Oceanography, Hohai University, Nanjing 210098, China
[2] State Key Laboratory of Simulation and Regulation of Water Cycle in River Catchment, China Institute of Water Resources and Hydropower Research, Beijing 100038, China
* Correspondence: yanping.li@hhu.edu.cn

Abstract: Large-scale irrigation can alter the regional water cycle process, which changes the structure and spatiotemporal distribution of local and downwind precipitation, impacting soil erosion in both the irrigated areas and the surrounding regions. However, the effects of large-scale irrigation on soil erosion in downwind vulnerable areas have not been investigated. The study used the high-resolution regional climate model (RegCM4) and the revised universal soil loss equation (RUSLE) to examine the effects of irrigation-induced precipitation in Northwest China on the frequency, distribution, and intensity of precipitation in the Yellow River Basin (YRB) under different Representative Concentration Pathways (RCPs). The response characteristics of soil erosion to the irrigation-induced precipitation effects and its relationship with slope, elevation, and land use type were analyzed as well. The results indicate that soil erosion in most regions of the YRB is below moderate, covering 84.57% of the basin. Irrigation leads to a 10% increase in summer precipitation indices (e.g., total wet-day precipitation, consecutive wet days, number of wet days with precipitation $\geq$ 1 mm, and number of heavy precipitation days with precipitation $\geq$ 12 mm) in the northwest of the basin. Irrigation also leads to a change in local circulation, resulting in reduced precipitation in the southeast of the basin, particularly under the RCP8.5 scenario. The transformation of erosion intensity between low-grade and high-grade erosion is relatively stable and small under the influence of precipitation. However, soil erosion changes display strong spatial heterogeneity, inter-annual and intra-annual fluctuations, and uncertainties. The findings of this study can be helpful for policymakers and water resource managers to better understand the impacts of large-scale irrigation on the environment and to develop sustainable water management strategies.

Keywords: large-scale irrigation; precipitation; soil erosion; regional climate model; Yellow River Basin

check for updates

Citation: Huang, Y.; Zhao, Y.; Li, G.; Yang, J.; Li, Y. Influence of Precipitation Effects Induced by Large-Scale Irrigation in Northwest China on Soil Erosion in the Yellow River Basin. *Remote Sens.* **2023**, *15*, 1736. https://doi.org/10.3390/rs15071736

Academic Editor: Guido D'Urso

Received: 8 February 2023
Revised: 21 March 2023
Accepted: 22 March 2023
Published: 23 March 2023

1. Introduction

Soil degradation caused by water erosion affects terrestrial ecosystems globally [1–3]. Global statistics show that 1.094 billion hm^2 of land is affected by water erosion, with 7.51 million hm^2 seriously impacted [4]. This results in soil nutrient loss, degradation, and a decline in productivity, exacerbating land scarcity [5]. Water erosion also causes the siltation of ditches and ponds, reducing their capacity for drainage and irrigation, leading to a decrease in agricultural productivity and an increase in floods, droughts, and other disasters. This further threatens the ecological environment, agricultural production, and social and economic sustainability [6,7]. Therefore, evaluating regional soil erosion intensity and its spatiotemporal distribution characteristics is of great significance for identifying key soil and water conservation areas and formulating corresponding measures.

China faces severe soil erosion, particularly in its arid and semi-arid areas [8]. The third Survey of Soil and Water Loss in China reports 5 billion tons of soil loss annually, with an average erosion intensity of 3800 $t{\cdot}km^{-2}{\cdot}a^{-1}$ in water-eroded areas. Soil and water loss has become one of the important factors restricting the steady development of China's economy and society. Arid and semi-arid regions' soil erosion is primarily driven by precipitation, particularly changes in extreme precipitation events [9]. Topsoil in these areas is particularly susceptible to erosion during floods, especially due to intensive agricultural activities and low vegetation cover [10,11]. In addition, Large-scale irrigation, which is often necessary for agriculture in China's arid and semi-arid regions, can impact the regional water budget and alter the patterns of extreme and seasonal precipitation, leading to changes in soil erosion's spatiotemporal distribution [12–14]. Mountainous and hilly regions with steep slopes and complex geological structures are particularly sensitive to soil erosion's changes in precipitation intensity, frequency, and distribution [15]. Despite the potential economic and ecological losses, there is little attention given to irrigation-induced precipitation effects on soil erosion's spatiotemporal distribution in these regions.

The Yellow River basin (YRB) is an important region in China, both economically and ecologically, providing significant output and essential services. Part of the YRB, the Loess Plateau, is one of the most severely affected areas of soil erosion globally due to its fragmented landform, high-intensity rainstorms, and human activities [16,17]. This erosion has led to decreased soil fertility, reduced surface vegetation, and a decline in land productivity [18]. At the same time, sediment deposition in the river causes the riverbed to continuously rise, resulting in floods and other disasters. Despite some studies estimating the state of soil erosion in the YRB, these have mainly focused on the current situation or small-scale areas [16,19–22]. Recent proposals suggest transferring the abundant water resources of Southwest China to the water-scarce regions of Northwest China, which could alleviate water shortages in agriculture and improve the fragile ecological environment [23,24]. As an important human agricultural activity, irrigation significantly impacts natural water cycling and the distribution of surface energy, inevitably affecting the regional climate through changes in land-atmosphere coupling, boundary layer processes, and precipitation system evolution [25]. Studies indicate that if this idea is implemented, large-scale irrigation in Northwest China will change the frequency, intensity, and spatiotemporal distribution of precipitation in the irrigated and surrounding areas [26]. However, the impacts of the precipitation effects produced by the proposed irrigation project on soil erosion have not been investigated in YRB. Due to the YRB's complex topography and vast area, directly measuring the impact of irrigation on soil erosion is difficult, expensive, and almost impossible. Therefore, understanding the impact of irrigation-induced precipitation effects on soil erosion with the help of numerical models is crucial for the YRB to develop future adaptation strategies and land plans.

The quantification of water erosion has gained worldwide attention [22,27]. Most studies on soil erosion have focused on small areas, such as slopes and small watersheds, using community experiments and mathematical models. The widely used models for quantifying water erosion include the Universal Soil Loss Equation (USLE) [28], the Water Erosion Prediction Project model (WEPP) [29], the revised universal soil loss equation (RUSLE) [30], and other models. RUSLE is widely recognized for its simplicity, compatibility with Geographic Information Systems (GIS), and efficiency, and it has been applied in various regions with different sizes and environmental conditions [31,32]. The RUSLE model considers factors such as rainfall, topography, vegetation, soil, and management measures and calculates the annual soil loss due to erosion through a factor-based method [33]. It has been well-applied in small and medium-sized regions or basins in China, such as the Loess Plateau, Bohai Rim, Hexi Corridor region, and Jiangxi Province [9,31,32,34]. However, there is limited attention given to large-scale watersheds. Thus, researchers in China have improved the RUSLE model's factor calculation method to make it more suitable for complex and broad areas. However, the default semi-empirical formulas used in RUSLE to calculate various factors, such as the Rainfall erosivity factor, Soil erodibility factor, and Topographic factor, cannot be applied to all regions with complex natural geographical and climatic features. Therefore, domestic researchers have improved the factor calculation method of the RUSLE model to make it more applicable to complex and vast regions [35,36]. Therefore, selecting suitable empirical calculation formulas for factors during the application of RUSLE is of great significance for ensuring the reliability of the results.

The study aims to assess the impact of large-scale irrigation on soil erosion in the YRB by using the RegCM4 model to dynamically downscale GCM products and applying the RUSLE model for water erosion assessment. The analysis will focus on comparing soil erosion patterns with and without irrigation and exploring the spatiotemporal variation of soil erosion in the region, taking into account different land use and land cover (LULC) types and geographical features. Section 2 will present the RegCM4 model, the RUSLE model, the preparation of data, and the methodology used. Section 3 will present the results of the climatic analysis and soil erosion under different geographical conditions. Section 4 will examine the potential factors driving changes in soil erosion patterns. Finally, Section 5 will summarize the key findings of the study, providing a theoretical basis for controlling soil erosion under the influence of climate change and large-scale irrigation and promoting soil conservation.

2. Data and Methodology

2.1. Data Preparation

The YRB constitutes an essential ecological and economic region in Northwest China (Figure 1). This region is not only an essential ecological corridor connecting China's three major plateaus (e.g., Loess Plateau, Qinghai-Tibet Plateau, and Inner Mongolia Plateau) and Huang-Huai-Hai Plain but also the area with the most severe soil erosion in China. The combined effects of low vegetation coverage, strongly erosive features of the loess soil, steep terrain, and frequent heavy rainfall in the flood season make the YRB one of the most erosive regions globally [16,17]. To explore the potential impact of large-scale irrigation-induced precipitation effects on soil erosion in the YRB, normalized vegetation index (NDVI), daily precipitation obtained from regional climate model simulations, soil type, a digital elevation model (DEM), and LULC types were used to calculate soil erosion.

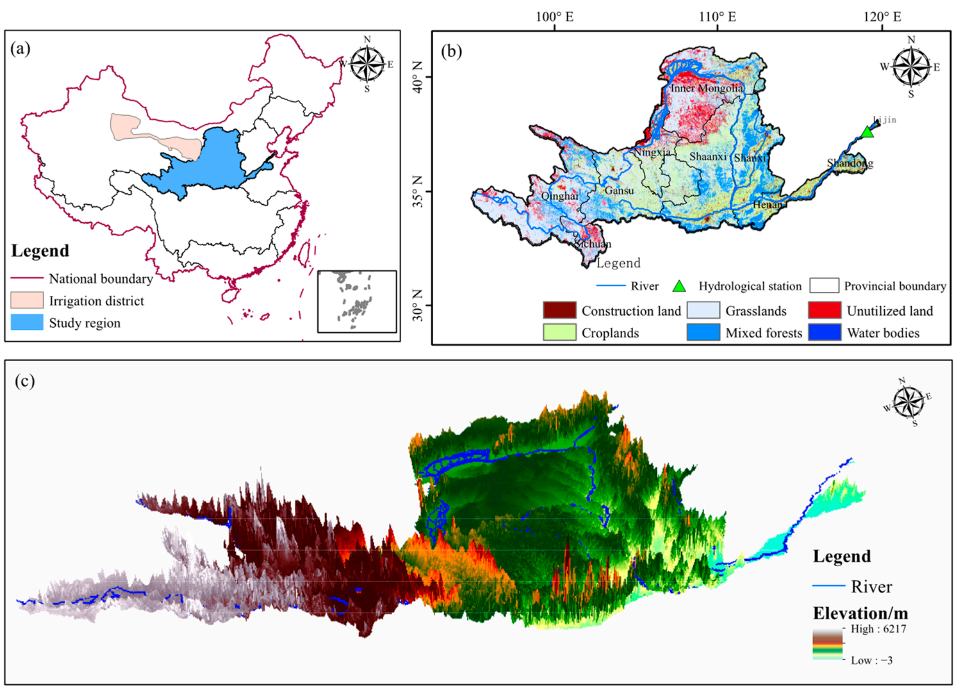

Figure 1. Location (**a**), LULC types (**b**), and terrain (**c**) of the YRB.

The precipitation data used in this study came from historical experiments conducted between 1970–2000 and future projections under the Representative Concentration Pathways (RCPs) (2020–2050) of the MPI-ESM-MR model [37]. The MPI-ESM-MR model was developed by the Max Planck Institute for Meteorology in Germany and has been extensively tested and evaluated against a range of observations and other models, showing good simulation performance for China [38,39]. MPI-ESM-MR provided the initial and lateral boundary conditions for the RegCM4 model to conduct dynamic downscaling simulations in the YRB. By switching irrigation schemes on and off in RegCM4, the regional climatology with and without irrigation were simulated (details in Section 2.2). To evaluate the performance of the RegCM4 model, the observed temperature and precipitation data from the CN05 dataset [40] with a resolution of 0.5° × 0.5° during the period of 1971–2000 was used. The topographic factor (LS) was calculated using a 90 m resolution DEM from the Shuttle Radar Topography Mission (https://srtm.csi.cgiar.org/ (accessed on 1 March 2023)). Other datasets used in the analysis, including LULC, NDVI, and soil data, were obtained from the Resource and Environment Science and Data Center (https://www.resdc.cn/ (accessed on 1 March 2023)), the International Soil Reference and Information Center (https://files.isric.org/soilgrids/latest/data/ (accessed on 1 March 2023)), respectively. All datasets were converted to a common map projection with a pixel size of 1 km for analysis.

2.2. Irrigation Scheme Description, Model Setup, and Numerical Experiments

The precipitation data was obtained by downscaling the MPI-ESM-MR historical (1971–2000) and future (2021–2050) results using the RegCM4 model developed by the International Center for Theoretical Physics in Italy [41]. RegCM4 is a regional climate model with a dimensional, hydrostatic, compressible, primitive equation and a σ-vertical coordinate. The model offers three different convection schemes (Kuo, Grell, Emanuel, Tiedtke, and Kain-Fritsch) for nonresolvable rainfall processes and three surface schemes (BATS, CLM3.5, and CLM4.5) to choose from. The study's selection of the RegCM4 model parameterization scheme was based on the findings of Gao et al. [42], which showed good performance in simulating the regional climate in China. Table S1 contains detailed information on the configuration of the scheme.

To obtain the regional precipitation under large-scale irrigation, we set the irrigation amount as the net rainfall reaching the topsoil after being intercepted by the vegetation canopy [43].

$$P_{net} = P_r + P_i + S_m - E \tag{1}$$

In Equation (1), P_{net} is the net rainfall that reaches the topsoil; P_r is precipitation; P_i is the irrigation amount; S_m is snow melt water; E is evapotranspiration. The water transfer mechanism was then coupled into the land surface model CLM3.5, which is the land surface component of RegCM4.

The study used precipitation simulation results with and without irrigation under RCP4.5 and RCP8.5 scenarios, based on the irrigation scenario assumption of Zhao et al. [26], to calculate soil erosion. The experimental design is presented in Table 1, with further details available from Zhao et al. [26]. Experiment 1 aims to verify the RegCM4's performance in simulating historical climatology. Experiments 2 and 4 are control experiments without irrigation under the RCP4.5 and RC8.5 scenarios, respectively. Experiments 3 and 5 are under the two RCPs but with irrigation. Among them, the precipitation from experiments 2–5 was used to calculate the rainfall erosivity factor in the RUSLE model. The RG_RF aimed to verify the RegCM4's ability to simulate historical climatology. Experiments N45 and N85 were control experiments conducted without irrigation under RCP4.5 and RCP8.5 scenarios, respectively. Experiments Y45 and Y85 were conducted under the two RCPs with irrigation. The precipitation data from experiments 2–5 was used to calculate the rainfall erosivity factor in the RUSLE model.

Table 1. Description of the irrigation experiment in this study.

Experiment	Scenario	Description
RG_RF	Historical	Default LULC type (without irrigation)
N45	RCP4.5	Default LULC type (without irrigation)
Y45	RCP4.5	The LULC type of the irrigated area is modified to crop (with irrigation)
N85	RCP8.5	Default LULC type (without irrigation)
Y85	RCP8.5	The LULC type of the irrigated area is modified to crop (with irrigation)

Notes: "N" and "Y" represent experiments with and without irrigation, respectively, and "45" and "85" indicate the RCP4.5 and RCP8.5 scenarios, respectively.

2.3. The RUSLE Model for Estimating Soil Erosion

The RUSLE was used to estimate the impact of irrigation-induced precipitation effects on the spatiotemporal pattern of soil erosion in the YRB.

$$A = R \times K \times LS \times C \times P \tag{2}$$

where A represents the annual soil erosion modulus per unit area (t·ha^{-2}·year^{-1}); K is the soil erodibility factor (t·h·MJ^{-1}·mm^{-1}); R is the rainfall erosivity factor (MJ·mm·ha^{2}·h^{-1}·a^{-1}); LS is the topographic factor; P and C stand for the soil conservation practice and the cover and management factors (dimensionless), respectively. Since this study focuses on the impact of irrigation-induced precipitation effects on soil erosion, K, LS, C, and P in the hypothesis formula, stay constant under different RCPs. The Soil erosion amounts are categorized into seven levels, from extremely severe (>150 t·ha^{-2}·year^{-1}) to very slight (<5 t·ha^{-2}·year^{-1}), based on the standard for classification and grading of soil erosion established by the Ministry of Water Resources, China [44].

2.3.1. Rainfall Erosivity Factor (R)

The rainfall erosivity factor (R, unit: MJ·mm·ha^{2}·h^{-1}·a^{-1}) is an important index reflecting the effect of rainfall on soil erosion. The Richardson daily precipitation erosivity estimation model modified by Zhang et al. [45] is used to calculate the R factor.

$$R_i = \alpha \sum_{j=1}^{k} (p_j)_i^{\beta} \tag{3}$$

where R_i represents the half-month rainfall erosivity; p_j represents the daily rainfall of day j-th of the i-th half month, which is required to be $\geq$12 mm [3,46]; i represents the i-th half month. The α and β are defined as follows:

$$\alpha = 21.568\beta^{-7.1891} \tag{4}$$

$$\beta = 0.8363 + \frac{18.177}{\overline{P}_{d12}} + \frac{24.455}{\overline{P}_{y12}} \tag{5}$$

where $\overline{P}_{d12}$ represents the average daily rainfall that is higher than 12 mm/day and $\overline{P}_{y12}$ represents the yearly average rainfall for days with rainfall higher than 12 mm/day. The precipitation data used in the calculation of the R-factor are all from the output results of the RegCM4 dynamic downscaling experiment in Table 1.

2.3.2. Soil Erodibility Factor (K)

The soil erodibility factor algorithm proposed by Wischmeier and Smith [28] is used to obtain the soil erodibility factor (K, unit: t·h·MJ^{-1}·mm^{-1}), which represents the sensitivity and rate of soil erosion.

$$K = [2.1 \times 10^{-4} M^{1.14}(12 - a) + 3.25(b - 2) + 2.5 \times (c - 3)] \times 0.1317/100 \tag{6}$$

$$M = (M_{\text{silt}} + M_{\text{vfs}}) \times (100 - M_{\text{c}}) \tag{7}$$

where a, b, and c are the organic matter content, soil structure grade, and soil saturation capability, respectively; M_{silt}, M_{vfs}, and M_{c} are the content of silt sand particles, very fine sand particles, and clay particles, respectively.

2.3.3. Topographic Factor (*LS*)

The topography factor (*LS*) is an essential factor inducing soil erosion and a necessary input parameter in constructing soil erosion models. The combined formula proposed by Liu et al. [35] and McCool et al. [47], which considers both gentle and steep slopes, is used to calculate the *LS*.

$$LS = L \cdot S \tag{8}$$

$$S = \begin{cases} 10.8\sin\theta, & \theta < 5^\circ \\ 16.8\sin\theta - 0.5, & 5^\circ \leq \theta < 10^\circ \\ 21.9\sin\theta - 0.96, & \theta \geq 10^\circ \end{cases} \tag{9}$$

$$L = (\lambda/22.13)^m \begin{cases} m = 0.5, \ \theta < 0.5^\circ \\ m = 0.4, \ 0.5^\circ \leq \theta < 1.5^\circ \\ m = 0.3, \ 1.5^\circ \leq \theta < 3^\circ \\ m = 0.2, \ \theta \geq 3^\circ \end{cases} \tag{10}$$

2.3.4. Cover and Management Factor (*C*)

Due to the close relationship between fraction vegetation cover (*FVC*) and *NDVI*, the regression algorithm proposed by Cai et al. [48] is used to calculate the coverage and management factor (*C*) under different *FVC*.

$$C = \begin{cases} 1, & FVC = 0 \\ 0.6508 - 0.343\log FVC, & 0 < FVC < 78.3\% \\ 0, & FVC \geq 78.3\% \end{cases} \tag{11}$$

$$FVC = \frac{NDVI - NDVI_{\min}}{NDVI_{\max} - NDVI_{\min}} \tag{12}$$

where *FVC* is the vegetation coverage (%); $NDVI_{\min}$ and $NDVI_{\max}$ represent the *NDVI* values corresponding to the cumulative probability of 5% and 95% of the pixels over the study region, respectively.

2.3.5. Soil Conservation Practice Factor (*P*)

The soil conservation practice factor (*P*) reflects the effectiveness of protective measures on surface soil and is closely linked to LULC types. According to the land classification characteristics of the YRB, the *p* values from previous studies were assigned to a dataset with a resolution of 1 km [9,16,31,33,49,50] (Table 2).

Table 2. Soil conservation practice factors based on LULC in the YRB.

p Value	LULC Types
1	Forest
0	Construction land
1	Bare soil
0.4	Dry cropland
0.01	Paddy field
1	Salinized land
1	Sandy land
0	Water bodies
1	Gobi Desert

Table 2. *Cont.*

p Value	LULC Types
1	Grassland
1	Marsh
0	Bare rock
1	Other types of unutilized land (alpine deserts and tundra, etc.)

3. Results

3.1. RegCM4 Performance for Climatology in YRB

The spatial distribution of precipitation simulated by the RegCM4 (Experiment RG_RF) is consistent with the observations from the CN05 dataset, but it has a wet bias, particularly in mountainous regions. As shown in Figure 2a, precipitation in the YRB displays a distinct geographical pattern with decreasing spatial pattern from south to north. The observed precipitation is primarily concentrated in the southern part of the YRB, with an average of less than 550 mm in most areas, while the observed multi-year average precipitation in the south is between 600 mm and 800 mm. The spatial correlation between the simulated precipitation and the observations in China is 0.56, and the observed multi-year average precipitation intensity is 1.69 mm/day (as shown in Table 3). In the YRB, the spatial correlation between the simulated precipitation and the observations is 0.83. However, the simulated multi-year average precipitation intensity of 3.05 mm/day is almost double that of the observed value.

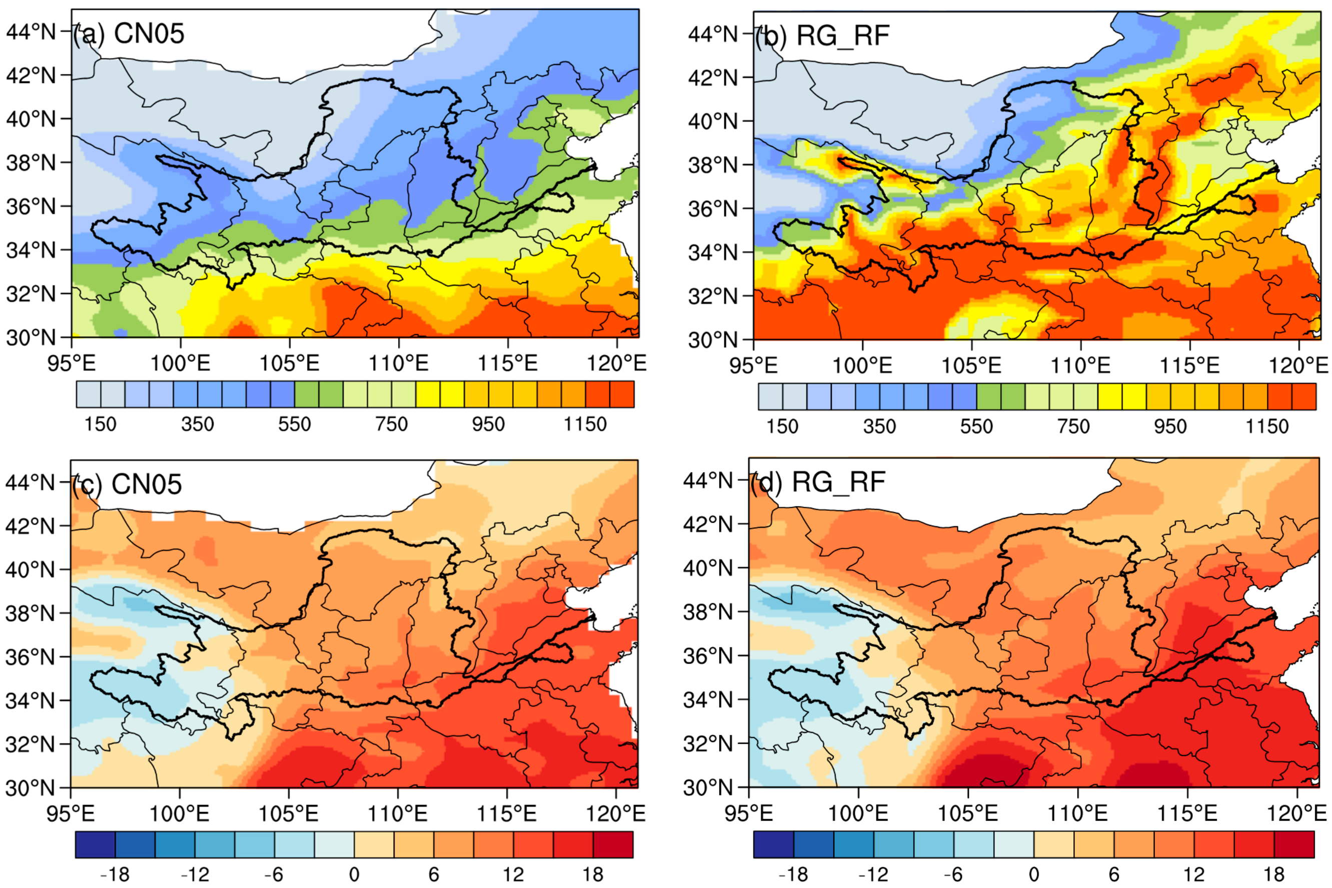

Figure 2. The observed and simulated multi-year average precipitation ((**a**): CN05; (**b**): RG_RF) and temperature ((**c**): CN05, (**d**): RG_RF) in the YRB.

Table 3. Performance parameters of the RegCM4 for precipitation and air temperature in China and the YRB.

		Precipitation		**Temperature**	
		Annual Average Precipitation (mm/day)	**Correlation Coefficient**	**Annual Average Temperature (°C)**	**Correlation Coefficient**
YRB	CN05	1.41		5.69	
	RG_RF	3.13	0.83	8.67	0.99
China	CN05	1.69		6.42	
	RG_RF	3.05	0.56	8.55	0.97

The performance of RegCM4 for air temperature in the region is better than for precipitation. The spatial distribution of temperature simulated by RegCM4 is almost consistent with observation, with a 2–3 °C warm bias overall (Figure 2c,d). The observed multi-year average air temperature in China is 6.42 °C and has a spatial correlation coefficient of 0.97 between observed and simulated air temperature (Table 3). In the YRB, the observed multi-year average temperature is around 5.69 °C, and the simulated air temperature has a spatial correlation of 0.99 with observation. Overall, although there are biases in precipitation and temperature, RegCM4 still has good performance in simulating the climatology of the YRB. The model can accurately capture the main spatiotemporal patterns of the observed precipitation and air temperature.

3.2. Spatial Pattern of the Factors Affecting Soil Erosion

The spatial pattern of the *R* factor under RCP4.5 without irrigation shows a significant increasing trend from the northwest to the southeast of the YRB, ranging from 89 to 37,064 $MJ\cdot mm\cdot ha^{-2}\cdot h^{-1}\cdot yr^{-1}$. The spatial pattern of the *R* factor under the RCP8.5 scenario is similar to that under the RCP4.5, but the values (126–37,878 $MJ\cdot mm\cdot ha^{-2}\cdot h^{-1}\cdot yr^{-1}$) are slightly larger. The spatial pattern of the *R* factor with irrigation is similar to that without irrigation (Figure S1). Figure 3c shows that the *K* factor ranges from 0.0178 to 0.0526 $t\cdot ha^{2}\cdot h\cdot ha^{-2}$ $MJ^{-1}\cdot mm^{-1}$, with the basin-average value of about 0.0388 $t\cdot ha^{2}\cdot h\cdot ha^{-2}$ $MJ^{-1}\cdot mm^{-1}$, which is close to that calculated by Sun et al. [16]. According to Figure 3c, the regions with the smallest *K* value are located in the central and western parts of Inner Mongolia, followed by the Qinghai region. Conversely, the regions with the highest *K* values are Ningxia and Gansu. Figure 3d demonstrates that higher *LS* values are typically found in mountainous areas with ridges, valleys, and steep slopes, which are more susceptible to erosion in the YRB. The lowest *LS* values are in flat regions, most of which are located in the northwest Inner Mongolia Loess Plateau, the south of the Loess Plateau in Shaanxi Province, and central Shanxi Province. As shown in Figure 3d, the *C* factor gradually decreases from northwest to southeast of the YRB. Areas with low *C* values are covered with forests and shrubs, mainly concentrated in the southeast and west parts of the YRB. Conversely, the maximum *C* values occur in Inner Mongolia and Ningxia, primarily on cultivated land and grassland. Human activities are widespread in the YRB, but the relevant soil conservation practices mainly occur in the farmland in the central and eastern valleys and plains of the YRB, where *p* values are relatively small (Figure 3f).

3.3. Variation in Soil Erosion Due to Irrigation-Induced Precipitation

According to the spatial pattern of soil erosion (Figure 4a,b), most regions in YRB have soil erosion rates below moderate intensity. These areas, accounting for 84.57% of the basin area, are mainly located in the source region of YRB, such as Ordos Plateau, Ningxia Plain, Hetao Plain, and Guanzhong Plain (Tables 4 and S2). On the other hand, regions with severe (4.84%), very severe (5.31%), and extremely severe (5.28%) soil erosion are mainly found in hilly, gully, and mountainous regions in Gansu, Ningxia, and northern Shanxi, where the terrain is rugged with steep slopes.

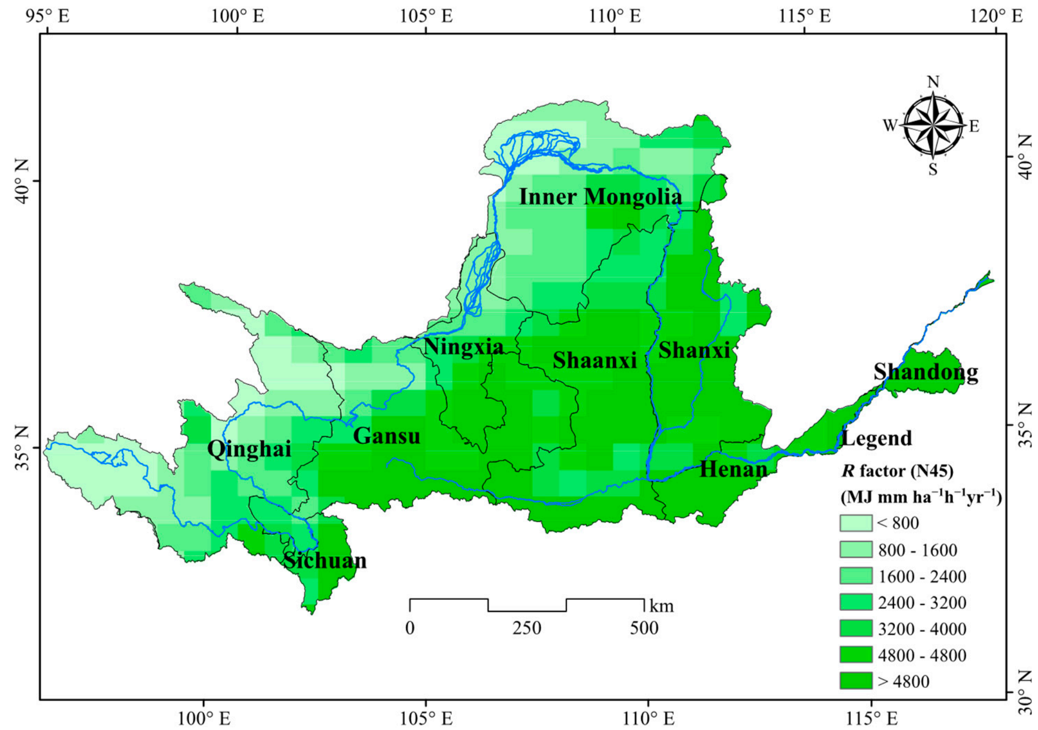

(**a**) *R* factor under N45

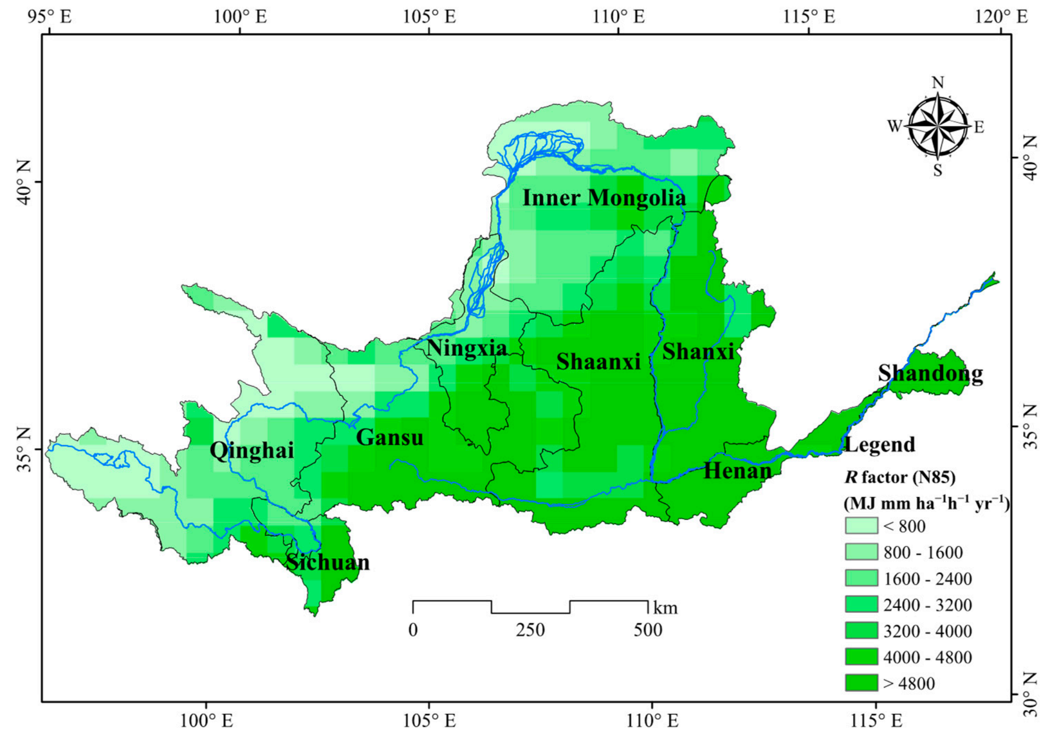

(**b**) *R* factor under N85

Figure 3. *Cont.*

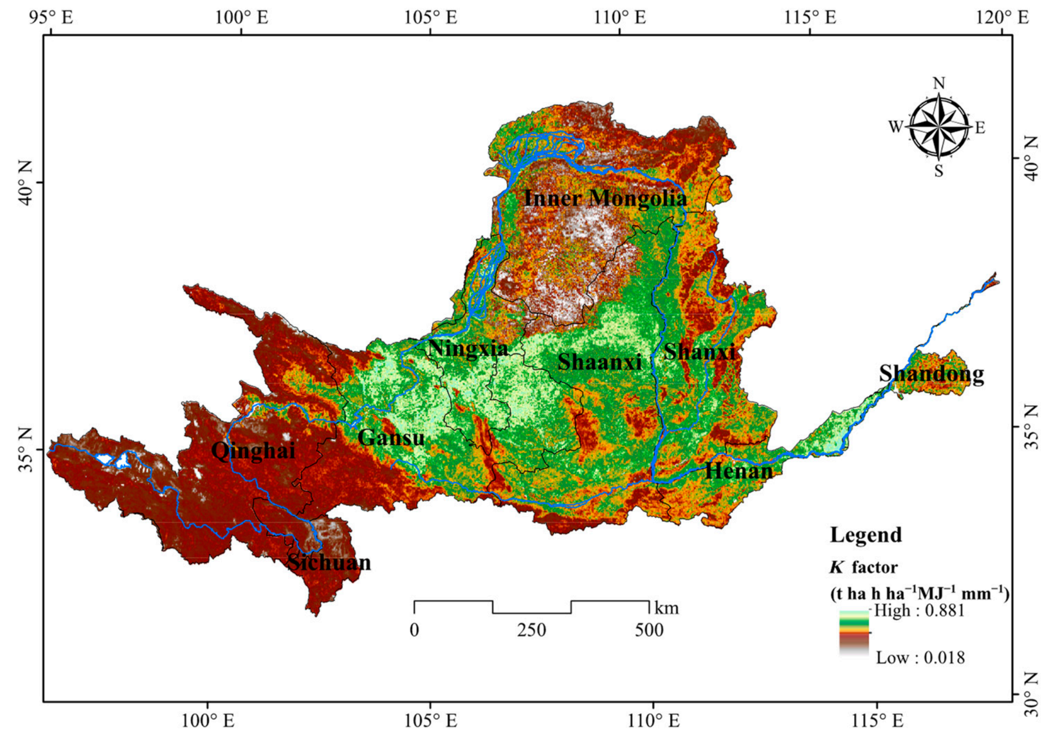

(**c**) *K* factor

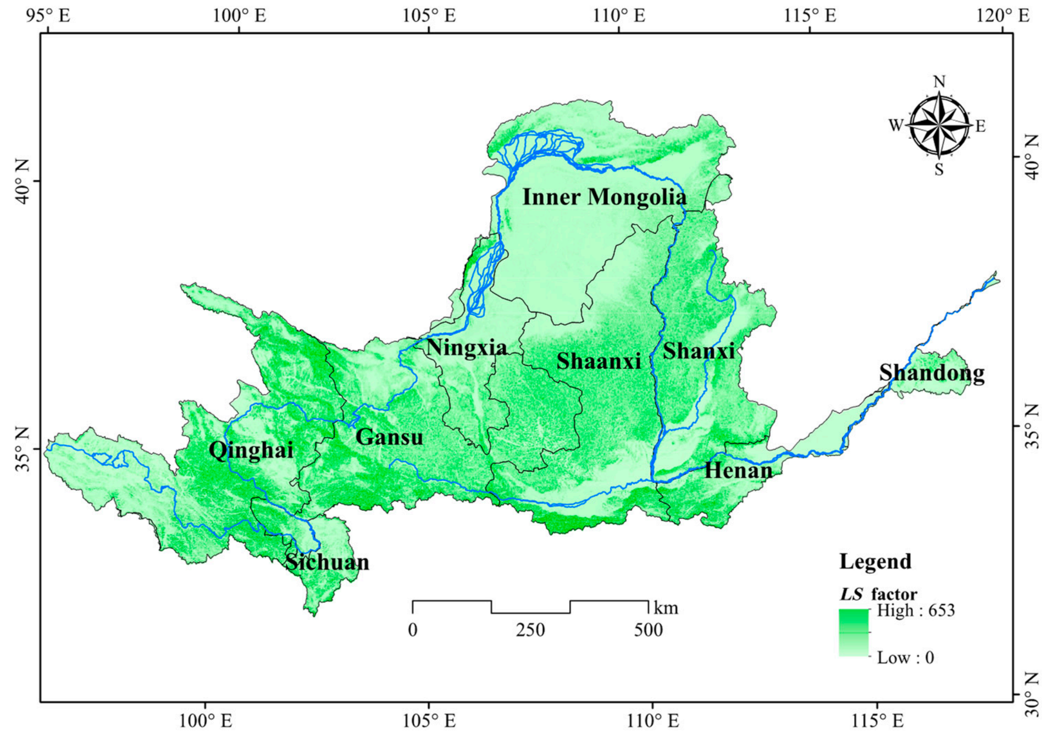

(**d**) *LS* factor

Figure 3. *Cont.*

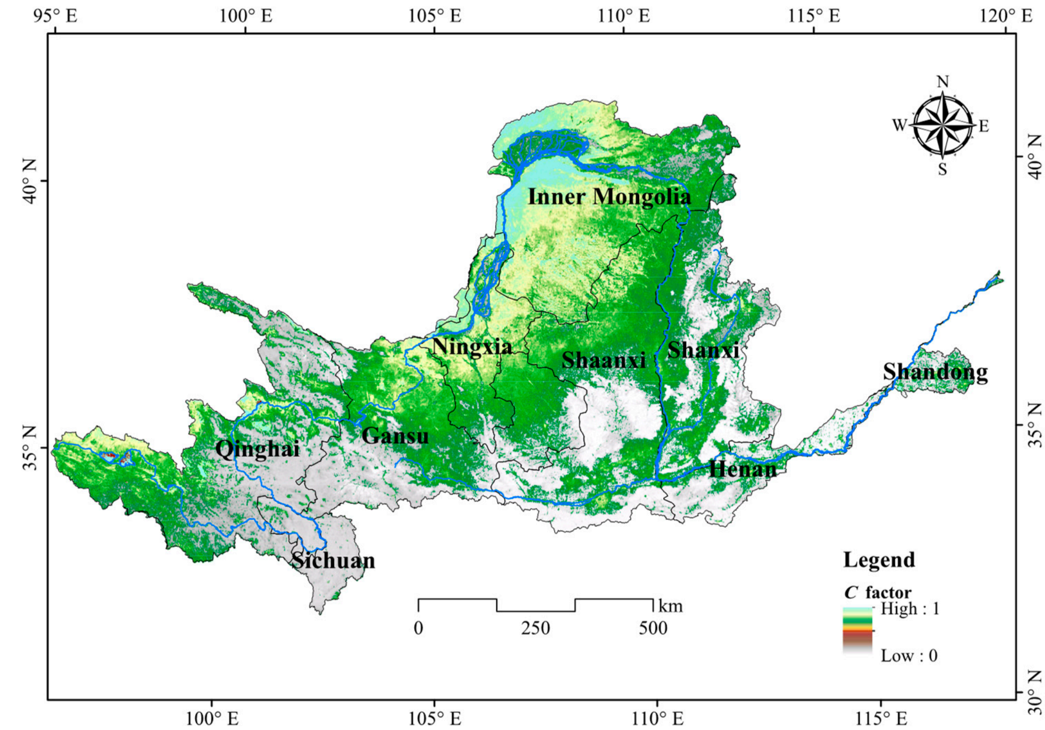

(**e**) *C* factor

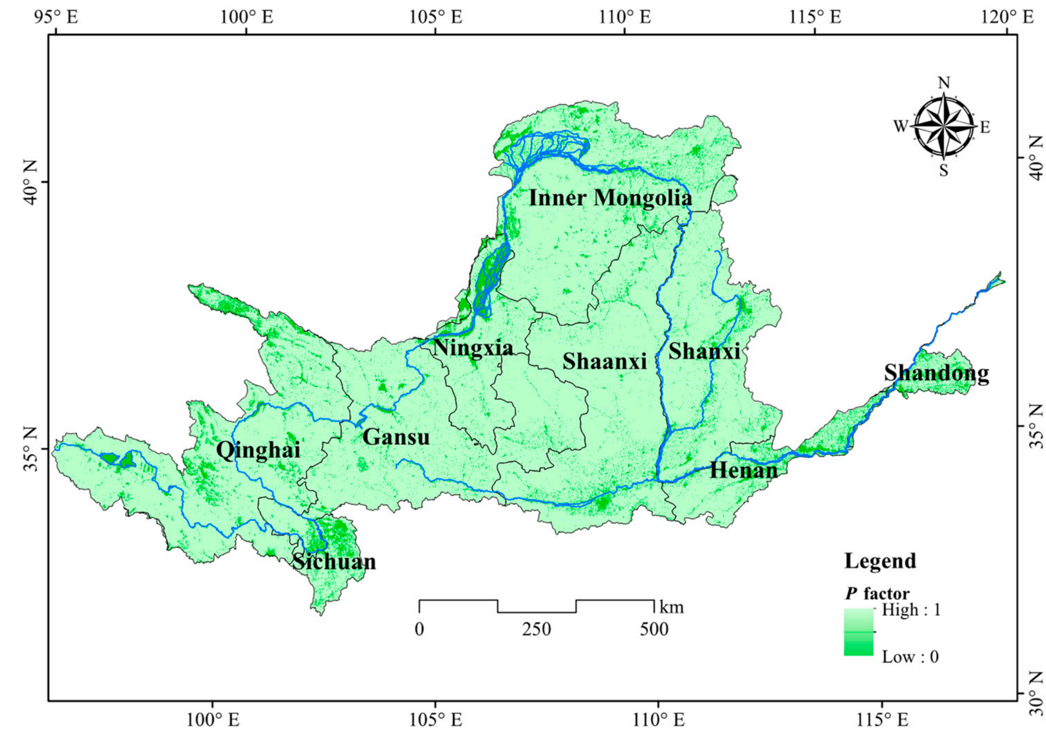

(**f**) *P* factor

Figure 3. Factors of the RUSLE model. (**a**,**b**) present the *R* factor under N45 and N85 scenarios; (**c**–**f**) *K*, *LS*, *C* and *P* factors in RUSLE model, respectively.

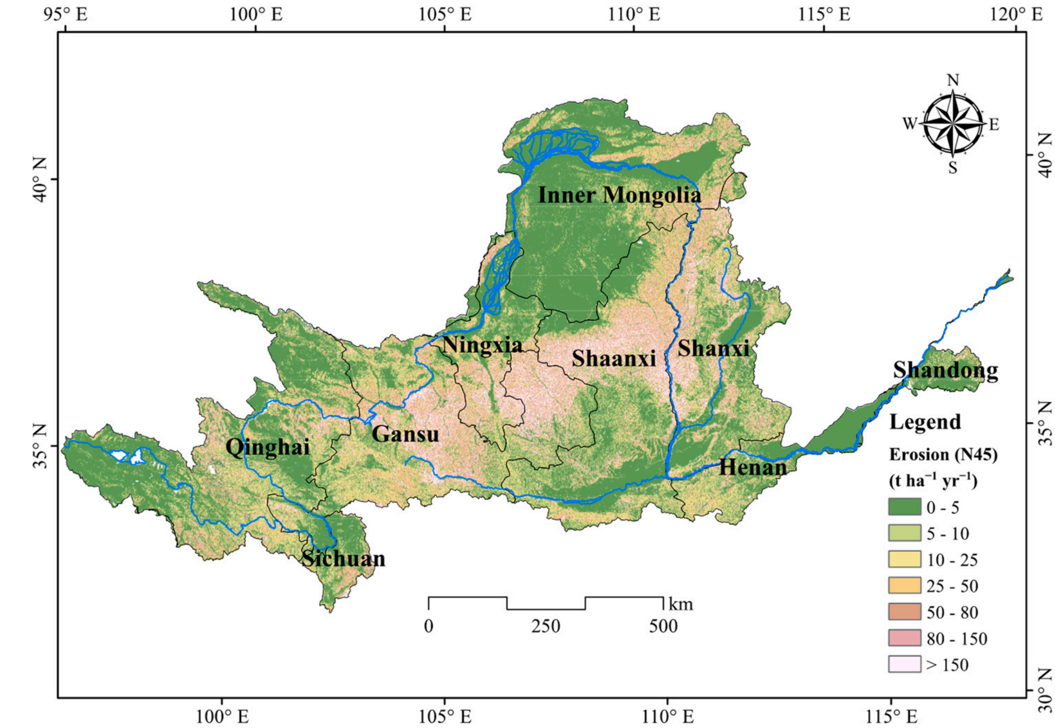

(**a**) soil erosion rate under N45

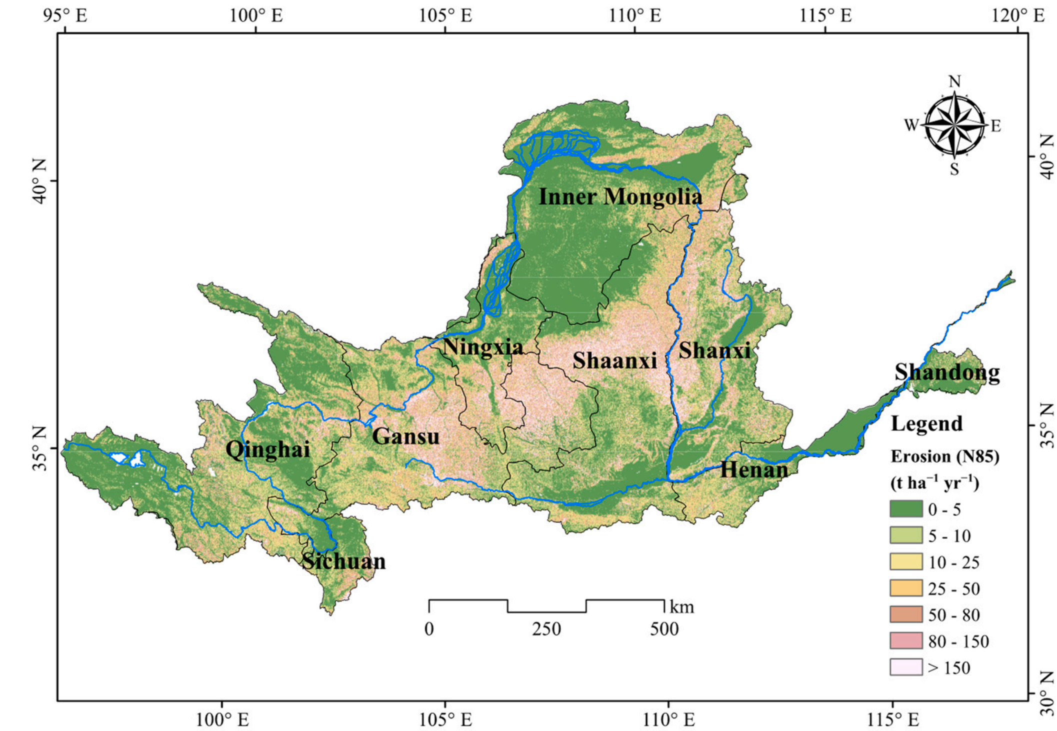

(**b**) soil erosion rate under N85

Figure 4. *Cont.*

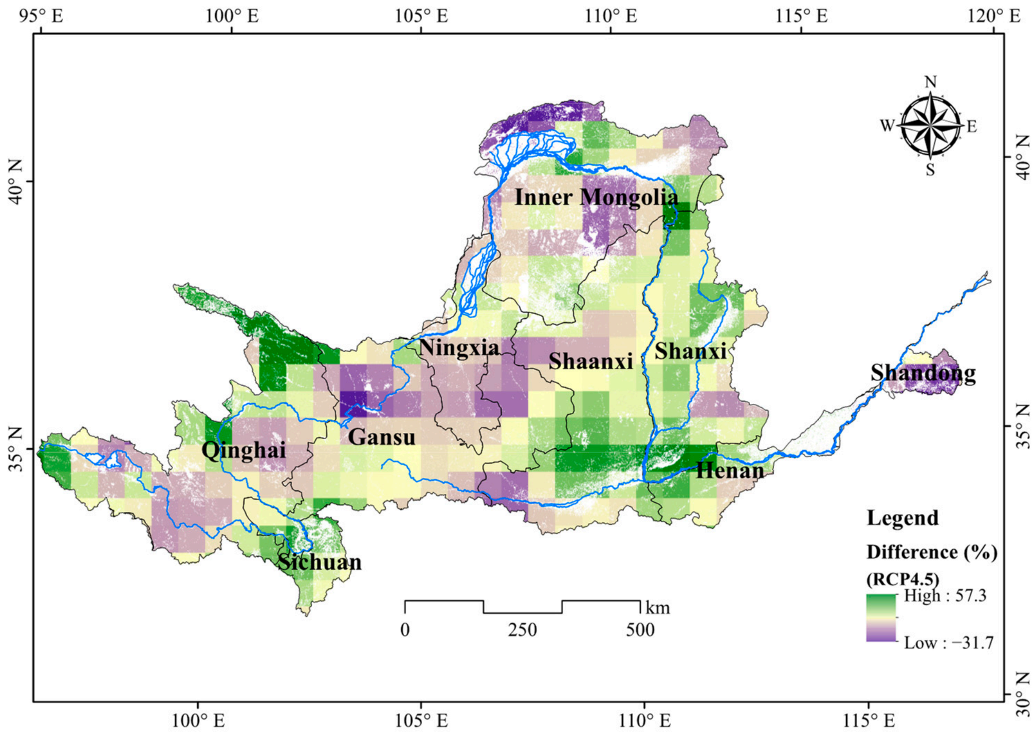

(**c**) Changes of soil erosion rate under RCP4.5

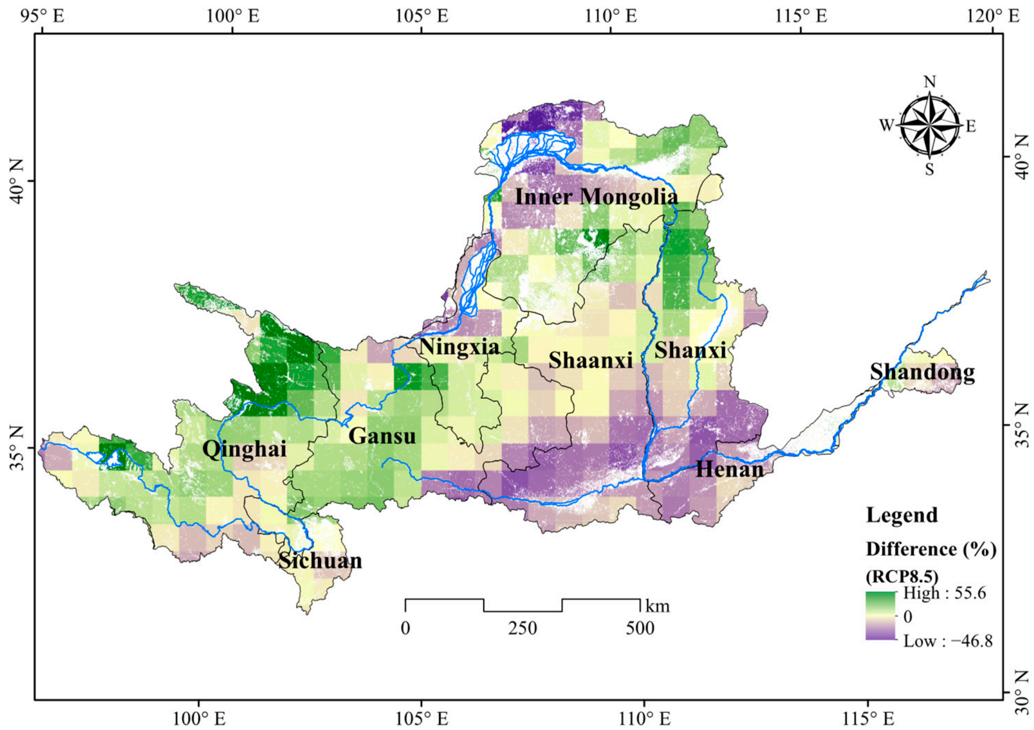

(**d**) Changes of soil erosion rate under RCP8.5

Figure 4. Spatial pattern of soil erosion rates in the YRB with and without irrigation. (**a**,**b**) depict the soil erosion rate in YRB under N45 and N85 experiments, respectively; (**c**,**d**) show the corresponding change rate (defined as $(Y - N) \times 100/N$), unit: %) of soil erosion rate with irrigation (Y45, Y85) compared to without irrigation (N45, N85).

Under the RCP4.5 and RCP8.5 scenarios, the multi-year basin-average soil erosion rates without irrigation are 17.48 and 18.05 $t{\cdot}ha^{-1}yr^{-1}$, respectively. With irrigation, the basin-wide soil erosion rate slightly decreases, and the multi-year average soil erosion rates under the RCP4.5 and RCP8.5 are 16.48 and 17.56 t·ha^{-1}yr^{-1}, respectively. Despite the decrease in basin average soil erosion rates under both scenarios, irrigation-induced precipitation change has a highly heterogeneous impact on soil erosion (Figure 4c,d). Under RCP4.5, most regions with increased soil erosion rates are in low-erosion areas, while decreased rates are found in high-erosion areas (Figure 4c). Under RCP8.5, however, the spatial variation of soil erosion rates is nearly the opposite of RCP4.5, and the increase (or decrease) of soil erosion rates is greater than under RCP4.5 (Figure S2). The standard deviation of soil erosion rate changes under the RCP4.5 and RCP8.5 is 10.21 and 12.63 t·ha^{-1}yr^{-1}, respectively, indicating a high spatial heterogeneity of soil erosion rate changes with the influence of irrigation-induced precipitation.

Table 4. Soil erosion transfer matrix with and without irrigation under RCP4.5 (%).

		Y45							
		Very Slight	Slight	Light	Moderate	Severe	Very Severe	Extremely Severe	Total
N45	Very slight	50.27	0.77						51.04
	Slight	0.53	9.92	0.76					11.20
	Light		0.56	12.83	0.56				13.95
	Moderate			0.48	7.47	0.38			8.34
	Severe				0.42	4.07	0.30		4.79
	Very severe					0.39	4.71	0.20	5.29
	Extremely severe						0.29	5.08	5.37
	Total	50.80	11.25	14.07	8.45	4.84	5.31	5.28	100.00

To further analyze the impact of irrigation-induced precipitation on the spatiotemporal characteristics of soil erosion in YRB under the two RCPs, a soil erosion transfer matrix is obtained by superimposing soil erosion areas with and without irrigation for RCP4.5 and RCP8.5 (Tables 4 and S2). Under RCP4.5, 94.32% of the watershed area saw no change in soil erosion area (Table 4). The area with low-grade erosion intensity that changed to high-grade erosion intensity is 2.97% of the YRB area, while the area with high-grade erosion intensity that changed to low-grade erosion intensity is 2.67%. The area where soil erosion is worsening is greater than the area where it is improving. Compared with RCP4.5, the soil erosion area of different grades under RCP8.5 is very close to that under RCP4.5 (Table S2). The area with low-grade erosion intensity that changed to high-grade erosion intensity is 2.52% of the YRB area, while the area with high-grade erosion intensity that changed to low-grade erosion intensity is 3.61%. The changes in soil erosion in YRB under different RCPs showed pronounced spatial heterogeneity under the influence of irrigation-induced precipitation effects. However, the transformation between low-grade and high-grade erosion intensity is relatively stable with only slight variation.

3.4. Soil Erosion Changes in Different LULC Types

The primary LUCC type in YRB is grassland, which covers 48.6% of the area, followed by farmland (25.1%). Other LULC types, such as forests, water bodies, construction land, bare rock, and undisturbed land, make up the remaining 26.3% (Table 5). In general, grasslands and forests tend to be located in mountainous regions with steep terrain and poor soil and water retention, which leads to higher soil erosion rates compared to other LULC types [51]. The region-average soil erosion rate for grasslands is 29.51 t·ha^{-1}yr^{-1}, and for dry cropland is 21.55 t·ha^{-1}yr^{-1}. The average soil erosion rate for forests and unutilized lands is 30.46 and 7.87 t·ha^{-1}yr^{-1}, respectively. The varying vegetation coverage causes significant soil erosion heterogeneity in different regions [52]. The influence of irrigation-induced precipitation leads to slight changes in soil erosion rate and area for all LULC types. Undisturbed land with weak erosion intensity and occupying a small proportion of YRB's area increases in both soil erosion intensity and area, especially in very severe and extremely severe regions. The grassland, the largest proportion of the YRB, shows a slight decrease and increase in the soil erosion rate under RCP4.5 (29.85 t·ha^{-1}yr^{-1}) and RCP8.5 (31.29 t·ha^{-1}yr^{-1}), respectively. Dry cropland, the second largest LULC type, shows a slight increase in soil erosion rates under both RCP4.5 (21.22 t·ha^{-1}yr^{-1}) and RCP8.5 (21.54 t·ha^{-1}yr^{-1}). In general, under RCP4.5, the erosion area slightly increases for forest, grassland, and dry cropland, except in regions with very slight, very severe, and extremely severe erosion. Under RCP8.5, the erosion area for dry cropland, forest, grassland, and unutilized land increases in extremely severe, very severe, severe, and very slight regions, while it mainly decreases in regions with slight, light, and moderate erosion.

Table 5. Soil erosion area percentage (%) of different LULC types.

LULC Type		**Very Slight**	**Slight**	**Light**	**Moderate**	**Severe**	**Very Severe**	**Extremely Severe**	**Total**
RCP4.5	Paddy field	0.74							0.74
	Dry cropland	13.27 (−0.43)	2.50 (0.84)	2.92 (0.99)	2.26 (1.47)	1.54 (0.22)	1.42 (−0.11)	0.50 (−4.29)	24.41
	Forest	4.98 (−2.98)	2.53 (0.96)	3.07 (1.97)	1.29 (2.76)	0.49 (4.65)	0.53 (−0.05)	0.65 (0.78)	13.53
	Grassland	20.36 (−0.24)	5.74 (0.14)	7.67 (0.46)	4.68 (0.90)	2.71 (1.15)	3.30 (0.38)	4.16 (−1.94)	48.61
	Water body	1.46							1.46
	Construction land	3.55							3.55
	Bare rock	1.38							1.38
	Unutilized land	5.31 (0.16)	0.44 (−0.86)	0.29 (−1.21)	0.12 (−0.11)	0.05 (−3.33)	0.05 (0.54)	0.05 (1.16)	6.31
RCP4.5	Paddy field	0.74							0.74
	Dry cropland	13.18 (0.71)	2.53 (−2.32)	2.96 (−2.32)	2.27 (0.24)	1.54 (0.24)	1.43 (1.91)	0.51 (−0.52)	24.41
	Forest	4.86 (0.50)	2.54 (0.33)	3.12 (−1.91)	1.30 (0.13)	0.51 (−0.95)	0.54 (0.99)	0.66 (3.77)	13.53
	Grassland	20.42 (−0.72)	5.78 (−0.36)	7.66 (−0.44)	4.67 (−0.33)	2.72 (0.41)	3.28 (1.76)	4.08 (3.62)	48.61
	Water body	1.46							1.46
	Construction land	3.55							3.55
	Bare rock	1.38							1.38
	Unutilized land	5.30 (0.19)	0.44 (−1.08)	0.30 (−2.72)	0.12 (−2.55)	0.05 (5.25)	0.05 (2.16)	0.05 (4.03)	6.31

Notes: The parentheses represent the percentage (%) change in soil erosion areas of different LULC types under the irrigation scenario.

3.5. Soil Erosion Changes under Different Topographic Conditions

To understand the impact of irrigation-induced precipitation on the soil erosion rate in the YRB, different altitude and slope zones were analyzed statistically (Table 6). The analysis of slope zones showed that the largest soil erosion area in the YRB is in the zone with a slope less than 5°, accounting for 49.04% of the basin area. This is followed by zones with slopes of 5–10°, 10–15°, 15–20°, and 20–25°, accounting for 21.42%, 15.5%, 8.51%, and 3.66% of the area, respectively. Zones with slopes greater than 25° only accounted for 1.87% of the area. Zones with high slopes are primarily located in the northeast-southwest hills and southeast mountainous regions. Soil erosion rates in all slope zones of the YRB are mainly moderate to mild. In the 0–5° slope zone, over 90% of the area had soil erosion grades below moderate, while 75–80% of the >20° and 5–20° slope zones had such grades. Under the influence of irrigation-induced precipitation, the soil erosion area of different slope levels increased or decreased slightly. In general, under RCP4.5, except for regions with very slight or extremely severe erosion, the soil erosion area increased at different slopes. Under RCP8.5, the soil erosion area decreased in regions with low-moderate erosion intensity but increased in regions with greater than severe erosion intensity.

Table 6. Soil erosion area percentage (%) of different slope zones.

Slope (°)		Very Slight	Slight	Light	Moderate	Severe	Very Severe	Extremely Severe	Total
RCP4.5	0°–5°	35.80(0.00)	4.06(0.45)	3.92(0.17)	2.10(−0.58)	1.13(−0.63)	1.08(0.25)	0.96(−0.74)	49.04
	5°–10°	6.69(−1.00)	2.93(0.47)	3.98(0.98)	2.64(1.45)	1.65(−0.01)	1.82(0.42)	1.71(−1.84)	21.42
	10°–15°	4.23(−1.90)	2.19(0.23)	3.04(1.37)	1.93(2.16)	1.16(2.46)	1.40(−0.16)	1.54(−2.22)	15.5
	15°–20°	2.42(−2.41)	1.25(0.45)	1.81(1.30)	1.00(2.87)	0.55(3.30)	0.67(0.00)	0.79(−2.21)	8.51
	20°–25°	1.10(−2.28)	0.55(0.32)	0.83(0.95)	0.47(2.51)	0.22(3.89)	0.23(0.11)	0.28(−1.79)	3.66
	>25	0.70(−1.90)	0.25(2.22)	0.40(0.73)	0.22(1.15)	0.10(1.45)	0.09(2.85)	0.11(−1.51)	1.87
RCP8.5	0°–5°	35.75(0.07)	4.09(−0.79)	3.92(−0.55)	2.11(−0.40)	1.14(−0.43)	1.09(1.86)	0.95(2.12)	49.04
	5°–10°	6.66(−0.39)	2.96(−1.01)	3.99(−1.20)	2.65(−0.12)	1.64(1.06)	1.83(1.52)	1.69(3.64)	21.42
	10°–15°	4.21(−0.26)	2.19(−0.42)	3.08(−1.82)	1.93(0.04)	1.18(−0.47)	1.39(2.02)	1.52(3.47)	15.5
	15°–20°	2.39(−0.15)	1.27(−0.52)	1.83(−1.36)	1.00(0.15)	0.56(0.02)	0.67(1.57)	0.78(2.93)	8.51
	20°–25°	1.09(−0.36)	0.56(−0.57)	0.84(−1.14)	0.47(−0.33)	0.22(2.18)	0.23(1.92)	0.27(3.33)	3.66
	>25	0.70(−0.38)	0.25(2.20)	0.41(−2.44)	0.22(−0.23)	0.10(1.19)	0.09(0.54)	0.10(5.85)	1.87

Notes: The parentheses represent the change percentage (%) in the soil erosion area in different slope zones under the irrigation scenario.

The areas of very severe and extremely severe soil erosion in the transitional zones between the Huang-Huai-Hai Plain (0–1000 m) and the Loess Plateau, as well as in the western mountainous area (>2000 m), are more sensitive to irrigation-induced precipitation effects than areas with soil erosion intensity below moderate (Table S3). Approximately 53.2% of the YRB, mainly the Loess Plateau, is located at 1000–2000 m, where serious soil erosion is present, and 82% of the area had soil erosion intensity below moderate to mild. In general, under RCP4.5, the soil erosion area increased in most elevation zones except for the low-altitude zone (<1000 m), with soil erosion intensity below moderate. Under RCP8.5, the soil erosion area decreased in low-altitude zones (<2000 m) but increased in high-altitude zones such as the western and southern alpine areas of the YRB. Note that under RCP8.5, erosion areas in high-altitude regions with soil erosion intensity above moderate increased more than under RCP4.5.

4. Discussion

Soil erosion in the YRB is complex and diverse and has been studied in terms of water erosion, wind erosion, and freeze-thaw erosion [53,54], but few studies have evaluated the effects of irrigation-induced precipitation on soil erosion despite many studies on the regional climate effects of irrigation [12–14]. In particular, little research has been conducted on the potential soil erosion risks in the YRB region and surrounding areas due to the irrigation-induced precipitation effects from envisaged (or planned) projects. Erosion intensity is related to topography, LULC changes, soil type and precipitation, and soil erosion from surface runoff erosion caused by heavy precipitation is the main source of river sediments [55]. When soil erosion in YRB is influenced by human activities, topography, and soil texture, it is especially sensitive to the spatiotemporal variation of precipitation [17,56]. The RegCM4 and RUSLE models were jointly used to simulate and analyze the precipitation effects of large-scale irrigation in Northwest China on soil erosion in YRB. This study is timely and necessary due to the increased risk of soil and land degradation in the YRB caused by changing climatic conditions and human activities, which may affect its unique biological diversity and ecology [19–21].

4.1. Links between Irrigation-Induced Changes in Precipitation Structure and Soil Erosion

Precipitation plays a key role in soil erosion, especially in this study, where all other factors in the RUSLE model, except the R factor, are considered static. Figure 5 and Figure S3 show the consecutive dry days (CDD), the percentage difference of summer total wet-day precipitation (PRCPTOT), consecutive wet days (CWD), the number of wet days with precipitation $\geq$ 1 mm (R01mm), the number of heavy precipitation days with precipitation $\geq$ 12 mm (R12mm), and the simple daily intensity index (SDII) with and without irrigation under RCP4.5 and RCP8.5, respectively. Figure 5 shows the summer precipitation indices (e.g., PRCPTOT, CWD, R01mm, and R12mm) with irrigation in the northwest YRB increase significantly ($p < 0.05$) by about 10%. Clearly, irrigation in northwest China has changed the precipitation structure of YRB, increasing the total effective precipitation events but reducing the average precipitation intensity (Figure 5). According to Equation (3), only precipitation events with precipitation intensity exceeding 12 mm/day can be used for the RUSLE model. The spatial heterogeneity of R12mm directly affects the spatial variation characteristics of soil erosion, and under the comprehensive influence of soil types, LULC, soil and water conservation measures, etc., soil erosion changes in the basin show high spatial heterogeneity, especially under the RCP8.5 (Figure S3). Except for the significant increase of R12mm with irrigation in the northwest of the YRB adjacent to the irrigated area, the basin shows no significant changes, and the variation is usually within 10% under the RCP4.5 and RCP8.5. However, even with such a small change in R12mm, the changes in soil erosion in some regions of the YRB reach about 50% (Figure 4c,d).

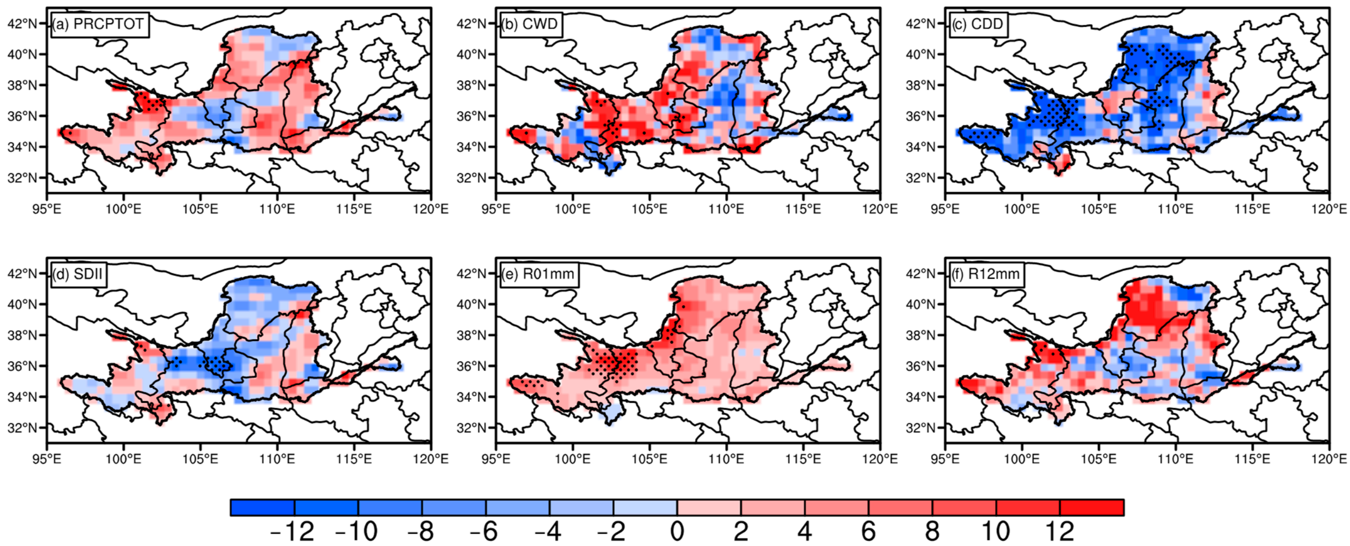

Figure 5. Spatial distribution of differences (defined as (Y − N) × 100/N; unit: %) in summer precipitation indices under RCP4.5 over the YRB. (**a**) PRCPTOT; (**b**) CWD; (**c**) CDD; (**d**) SDII; (**e**) R01mm; (**f**) R12mm.

Figure 6 shows the circulation differences in the YRB and its surrounding areas from June to August with and without irrigation under the RCP8.5. As shown in Figure 6a–c, a local anticyclonic anomaly is generated in the center of the irrigation area, which enhances westerly winds north of the irrigation region and a southerly wind moving away from the irrigation region. This circulation perturbation leads to downstream circulation anomalies, including a cyclonic anomaly in central China. In July, this anomaly enhances monsoonal flow—an anticyclonic anomaly further along the interface between a subtropical high and westerly flow. The strength and location of the seasonal circulation anomaly are sensitive to the configuration of the original circulation. In July, compared to June and August, westerly and northerly winds increase in areas surrounding the irrigation region, leading to less precipitation in the southeast YRB (Figure S3). Anticyclones are also present in the RCP4.5 but are not evident from June to August. This inconsistency in circulation variation between the RCP4.5 and RCP8.5 with and without irrigation contributes to differences in precipitation variation in the southeast YRB to a certain extent (Figure S4). Additionally, the circulation difference between RCP4.5 and RCP8.5 without irrigation also contributes to the spatial differences in precipitation changes. Comparing RCP4.5 and RCP8.5 without irrigation, we found that RCP8.5 has stronger southwesterly winds and an anticyclonic anomaly centered on the Mongolian Plateau in the East Asian Monsoon region, particularly in July (Figure S5). These differences correspond to a stronger East Asian Summer Monsoon in RCP8.5 than in RCP4.5. For the above reasons, the spatial difference in precipitation caused by irrigation is more significant under the RCP8.5 compared to the RCP4.5, a difference that further affects the spatial pattern of soil erosion.

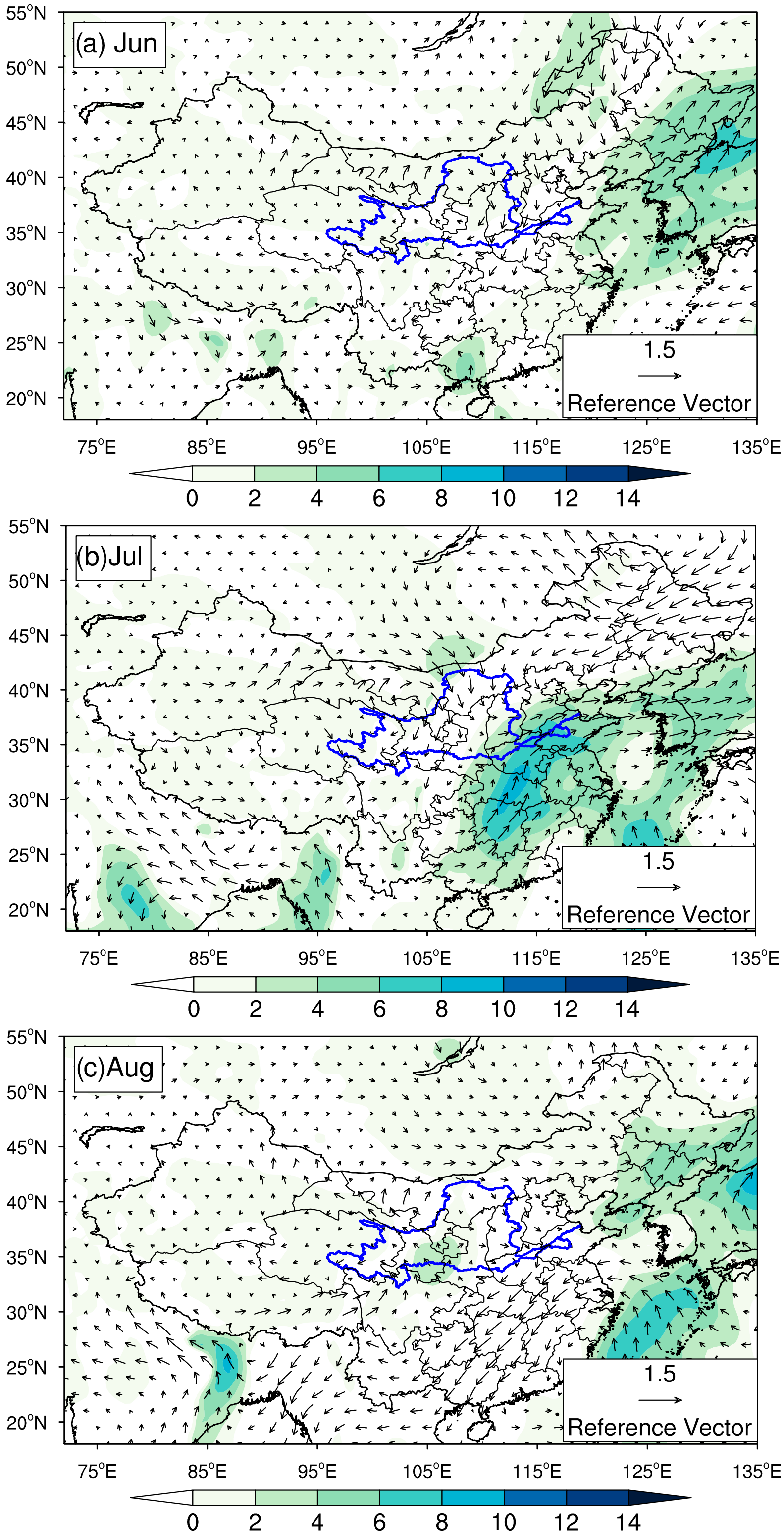

Figure 6. Differences (defined as Y minus N) in the integrated water vapor flux (shading, unit: kg·m^{-1}·s^{-1}) and wind field (vector, unit: m·s^{-1}) at 850 hPa under RCP8.5 from June to August. (**a**) June; (**b**) July; (**c**) August.

4.2. Soil Erosion Variability under Different RCP Scenarios with Large-Scale Irrigation

The effect of large-scale irrigation in northwest China on soil erosion in the YRB is generally small from a climatological and basin-average perspective. However, there are significant differences in YRB's soil erosion variability on annual and interannual scales. On an annual scale, irrigation activities in either the RCP4.5 or RCP8.5 mainly affect precipitation during the YRB flood season (June–October), with strong uncertainty (Figure 7). Guo et al. [57] found that during the flood season, the water volume of Lijin Station accounts for about 65% of the volume for the year and that the sediment volume accounts for over 80% of the year's volume. Nearly 90% of the sediments come from the middle reaches of the YRB, and the sediment load in the upper reaches only accounts for 10% of the total watershed [58,59]. Wang et al. [60] showed that the constructed wetland area in the Yellow River delta is negatively correlated ($R = -0.84$) with sediment transport at the Lijin Station, while the natural wetland in the estuary is positively correlated ($R = 0.6$) with the Lijin station's sediment load. Therefore, precipitation changes during the flood season may directly affect soil erosion and changes in water and sediment, leading to alternating siltation and scouring in the lower reaches of the YRB, which in turn affects the estuary delta's wetland area.

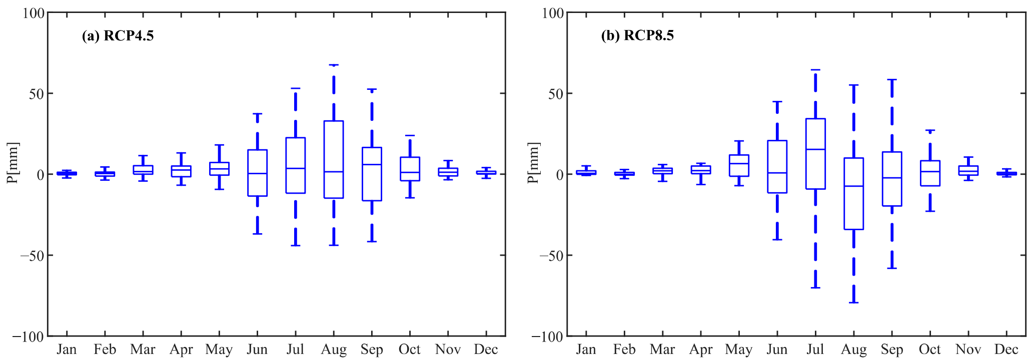

Figure 7. Variation of monthly precipitation with irrigation under the RCP4.5 (**a**) and RCP8.5 (**b**).

In addition, the interannual variation of soil erosion varies substantially under the influence of irrigation. On a basin-average level, the soil erosion rates of the normal and dry years are very low (<5 t·ha^{-1}yr^{-1}), while only wet years show rates higher than 10 t·ha^{-1}yr^{-1} (Table S4). In the high-intensity erosion areas in the YRB, soil erosion is usually strongly affected by the effects of irrigation. The overall change in soil erosion, as influenced by irrigation-induced precipitation effects, is stronger under RCP8.5 than under RCP4.5 and has a stronger spatial heterogeneity, as per standard deviation (Figure S6 and Table S4). If policies related to human activities are not considered, our study shows that sediment transport in the middle and lower reaches of the YRB is more likely to increase under RCP8.5 than under RCP4.5, potentially affecting the Yellow River delta.

4.3. Limitations and Future Work

The study has several limitations and shortcomings that may affect the interpretation of the results. Firstly, this study assumed that factors such as *K*, *LS*, *C*, and *P* did not change over time, but in reality, these factors are dynamic. It is important to acknowledge that the factors influencing soil erosion, such as *K*, *LS*, *C*, and *P*, are dynamic and can change over time. Agricultural activities, such as tillage, grazing, and deforestation, can significantly impact soil properties, which can lead to changes in the soil's erodibility (*K*) and subsequently affect soil erosion rates [61–63]. For example, tillage practices can cause soil compaction, decreased organic matter content, and increased exposure to the elements, all of which can increase soil erosion rates. Similarly, overgrazing and deforestation can lead to the loss of vegetation cover, which can also contribute to increased soil erosion rates. In addition, climate change can also affect soil erosion through its impact on vegetation cover

(*C*). As temperatures rise and precipitation patterns change, plant growth, and distribution can be altered, leading to changes in vegetation cover that can either increase or decrease soil erosion rates depending on the location and conditions [64,65]. Recently, some studies have found that the Yellow River basin is showing a warming and drying trend in the future [66], and changes in extreme weather events, such as extreme precipitation and drought within the basin, will have a significant impact on soil erosion [66–68]. Additionally, various effective measures (*P*) to control soil erosion have been implemented in China, including implementing conservation tillage practices, building terraces, and implementing grassland and forest conservation programs, which play a crucial role in mitigating soil erosion [69,70]. Overall, understanding the complex relationships between these factors is important for developing effective strategies to mitigate soil erosion and promote sustainable land use practices.

Secondly, the quality and accuracy of data have limited quantitative research. The MPI-ESM-MR model-forced RegCM4 precipitation simulation has clear wet biases compared to observations, which may lead to overestimated soil erosion intensity due to increased false effective precipitation events (>12 mm/day) [71]. High-resolution data sets are necessary to analyze spatial variability of soil erosion intensity changes, but this study used bilinear interpolation to unify data with different resolutions into a grid for RUSLE model calculations, which limits the analysis of subtle changes in soil erosion. Although this study did not verify the accuracy of simulated soil erosion intensity with observational data, the overall simulation of soil erosion intensity and its spatial distribution are consistent with the previous study [16,72]. In the future, more precise data, rigorous methods, and ideal models will be used to further explore the potential effects and mechanisms of regional climate impacts induced by irrigation on soil erosion.

Finally, the assessment of the impact of regional climate effects caused by irrigation on soil erosion is uncertain due to the use of different climate models, regional models, study periods, and emission scenarios [73]. Cheng et al. [5] found that the R-factors calculated by different RCPs and GCMs in the same region differ significantly. Using the average composite of 19 global climate models, Panagos et al. [74] predicted future rainfall erosivity for three representative concentration pathways (RCP2. 6, RCP4.5, and RCP8.5) and observed significant variations in soil erosion intensity and spatial distribution across different climate backgrounds. Our study only evaluated soil erosion changes under RCP4.5 and RCP8.5 in the MPI-ESM-MR, but there are significant spatial differences between the two, indicating high uncertainty in the impact of irrigation-induced precipitation on soil erosion in the YRB due to the complex atmospheric circulation and precipitation responses. Additionally, the study's estimate of 60 billion m^3 of water used is based on the results of a hypothetical representative scheme in the water transfer irrigation of Northwest China, which is still controversial and has not been scientifically proven [26]. Therefore, the study's evaluation of the impact of large-scale irrigation in Northwest China on soil erosion in the YRB is specific to the models, scenarios, methods, and irrigation amounts used.

5. Conclusions

Large-scale irrigation has been shown to impact regional precipitation frequency, intensity, and spatiotemporal patterns, making it important to assess its impact on soil erosion in the YRB. In the study, the RegCM4 and the RUSLE model were jointly used to analyze the impact of precipitation caused by large-scale irrigation in Northwest China on soil erosion in the YRB under different RCPs. The relationship between soil erosion intensity and different slopes, LULC types, and altitudes was analyzed. Another discussed topic was the relationship between soil erosion and water and sediment changes. The main findings are as follows:

(1) 84.57% of the YRB is characterized by below-moderate soil erosion, with the main zones of soil erosion located in grassland regions with an altitude of 1000–2000 m and a slope of less than 5°. Areas of severe, very severe, and extremely severe soil erosion

are mainly found in Gansu, Ningxia, and northern Shanxi, where fragmented terrain features ridges and valleys with steep slopes.

(2) Irrigation in northwest China has impacted the pattern and distribution of precipitation in the YRB, primarily in the northwest regions near the irrigation area. The irrigation causes a rise in summer precipitation indices (e.g., PRCPTOT, CWD, R01mm, and R12mm) in the northwest of the basin. It also leads to a change in local circulation, resulting in reduced precipitation in the southeast of the basin, particularly under the RCP8.5 scenario.

(3) The effects of irrigation-induced precipitation on soil erosion intensity in the YRB are slight but amplify the spatial heterogeneity of soil erosion by superimposing non-climate factors such as land use, soil type, and human activities, particularly in vulnerable regions. The change in erosion intensity between low-grade and high-grade erosion is relatively stable and small, but soil erosion changes display high spatial heterogeneity, inter-annual and intra-annual fluctuations, and uncertainties. Under the RCP8.5 scenario, the characteristics of soil erosion change are almost the opposite of those under RCP4.5, with a greater variation amplitude.

In summary, this study emphasizes the importance of considering the impact of irrigation-induced precipitation effects on soil erosion in the YRB and the necessity for policymakers and land managers to develop adaptation strategies to address these challenges. Evaluating the impact of large-scale irrigation-induced precipitation on soil erosion in the YRB is critical to inform and support adaptation strategies. The influence of irrigation on soil erosion may vary in different climate conditions and natural geographical features. Hence, it is essential to consider local conditions when devising adaptation strategies to reduce soil erosion. By implementing measures such as changing irrigation methods, adopting conservation tillage, afforestation, and improving soil quality, policymakers and land managers can mitigate the risk of soil erosion and ensure the sustainability of agriculture in the YRB.

Supplementary Materials: The following supporting information can be downloaded at: https://www.mdpi.com/article/10.3390/rs15071736/s1. Table S1: The RegCM4 Model configuration used in this study. Table S2: Transfer matrix of soil erosion rate before and after irrigation under RCP8.5 scenario (%). Table S3: Soil erosion area percentage (%) in different altitude zones. Table S4: Statistical parameters of soil erosion change in typical years. Figure S1: *R* factor (unit: $MJ \cdot mm \cdot ha^{-2} \cdot h^{-1} \cdot yr^{-1}$) of the RUSLE model under Y4.5 (a) and Y8.5 (b). Figure S2: Spatial pattern of soil erosion rates in the YRB with and without irrigation. [(a) and (b) depict the soil erosion rate in YRB under Y45 and Y85 experiments, respectively; (c) and (d) show the corresponding change rate (defined as Y−N), unit: $t \cdot ha^{-1} yr^{-1}$) of soil erosion rate with irrigation (Y45, Y85) compared to without irrigation (N45, N85)]. Figure S3: Spatial distribution of differences (defined as $(Y - N) \times 100/N$; unit: %) in summer precipitation indices under RCP8.5 over the YRB. [(a) PRCPTOT; (b) CWD; (c) CDD; (d) SDII; (e) R01mm; (f) R12mm]. Figure S4: Differences (defined as Y minus N) in the integrated water vapor flux (shading, unit: $kg \cdot m^{-1} \cdot s^{-1}$) and wind field (vector, unit: $m \cdot s^{-1}$) at 850 hPa under RCP4.5 from June to August. [(a) June; (b) July; (c) August]. Figure S5: Differences (defined as RCP8.5 minus RCP4.5) in the integrated water vapor flux (shading, unit: $kg \cdot m^{-1} \cdot s^{-1}$) and wind field (vector, unit: $m \cdot s^{-1}$) at 850 hPa from June to August. [(a) June; (b) July; (c) August]. Figure S6: Spatial distribution of soil erosion rate changes (defined as Y minus N; unit: $t \cdot ha^{-1} yr^{-1}$) in typical years. [(a)~(c) represent wet, dry, normal years under the RCP4.5 scenario, respectively; (d)~(f) are similar to (a)~(c), but under the RCP8.5 scenario].

Author Contributions: Y.H. designed the study, completed the original draft. Y.Z. provided financial support for the research. G.L. provided some software for the study. J.Y. analyzed the data. Y.L. revised the original draft. All authors commented on the manuscript and agreed to the published version of the manuscript. All authors have read and agreed to the published version of the manuscript.

Funding: The study was funded by the National Key Research and Development Program of China (2021YFC3200204), the Open Research Fund of State Key Laboratory of Simulation and Regulation of Water Cycle in River Basin, China Institute of Water Resources and Hydropower Research (IWHR-

SKL-KF202204), the Jiangsu Funding Program for Excellent Postdoctoral Talent (2022ZB147), the Key Scientific and Technological Project of the Ministry of Water Resources. P.R.C (SKS-2022001), the Systematic Project of Guangxi Key Laboratory of Disaster Prevention and Engineering Safety (2022ZDK026) and TianHe Qingsuo Project special fund project in the field of climate, meteorology and ocean.

Data Availability Statement: All the data are freely available. The MPI-ESM-MR forcing data from the International Center for Theoretical Physics (http://clima-dods.ictp.it/Data/RegCM_Data/ (accessed on 1 March 2023)). The CN05 observation data from Climate Change Research Center, Chinese Academy of Sciences (https://ccrc.iap.ac.cn/resource/detail?id=228 (accessed on 1 March 2023)). The 90m resolution DEM from the Shuttle Radar Topography Mission (https://srtm.csi.cgiar.org/ (accessed on 1 March 2023)). Other datasets used in the analysis, including LULC, NDVI, and soil data, were obtained from the Resource and Environment Science and Data Center (https://www.resdc.cn/ (accessed on 1 March 2023)), the International Soil Reference and Information Center (https://files.isric.org/soilgrids/latest/data/ (accessed on 1 March 2023)), respectively.

Acknowledgments: The authors greatly appreciate the data availability and service provided by China Meteorological Administration and the RegCM4 science team.

Conflicts of Interest: The authors declare no conflict of interest.

References

1. Chappell, A.; Baldock, J.; Sanderman, J. The global significance of omitting soil erosion from soil organic carbon cycling schemes. *Nat. Clim. Chang.* **2016**, *2*, 187–191. [CrossRef]
2. Zhang, S.-H.; Fan, W.-W.; Li, Y.-Q.; Yi, Y.-J. The influence of changes in land use and landscape patterns on soil erosion in a watershed. *Sci. Total Environ.* **2017**, *574*, 34–45. [CrossRef] [PubMed]
3. Teng, H.-F.; Liang, Z.-Z.; Chen, S.-C.; Liu, Y.; Rossel, R.-A.-V.; Chappell, A.; Yu, W.; Shi, Z. Current and future assessments of soil erosion by water on the Tibetan Plateau based on RUSLE and CMIP5 climate models. *Sci. Total Environ.* **2018**, *635*, 673–686. [CrossRef] [PubMed]
4. Lal, R. Soil erosion and the global carbon budget. *Environ. Int.* **2003**, *4*, 437–450. [CrossRef]
5. Cheng, Y.-T.; Li, P.; Xu, G.-C.; Li, Z.-B.; Gao, H.-D.; Zhao, B.-H.; Wang, T.; Wang, F.-C.; Cheng, S.-D. Effects of soil erosion and land use on spatial distribution of soil total phosphorus in a small watershed on the Loess Plateau, China. *Soil Tillage Res.* **2018**, *184*, 142–152. [CrossRef]
6. Van Pelt, R.-S.; Hushmurodov, S.-X.; Baumhardt, R.-L.; Chappell, A.; Nearing, M.-A.; Polyakov, V.-O.; Strack, J.-E.; Nearing, M.-A.; Baffaut, C. The reduction of partitioned wind and water erosion by conservation agriculture. *Catena* **2017**, *148*, 160–167. [CrossRef]
7. Hata, K.-J.; Osawa, T.; Hiradate, S.; Kachi, N. Soil erosion alters soil chemical properties and limits grassland plant establishment on an oceanic island even after goat eradication. *Restor. Ecol.* **2019**, *2*, 333–342. [CrossRef]
8. Moghadam, B.-K.; Jabarifar, M.; Bagheri, M.; Shahbazi, E. Effects of land use change on soil splash erosion in the semi-arid region of Iran. *Geoderma* **2015**, *241–242*, 210–220. [CrossRef]
9. Lin, J.-K.; Guan, Q.-Y.; Tian, J.; Wang, Q.-Z.; Tan, Z.; Li, Z.-J.; Wang, N. Assessing temporal trends of soil erosion and sediment redistribution in the Hexi Corridor region using the integrated RUSLE-TLSD model. *Catena* **2020**, *195*, 104756. [CrossRef]
10. Cantón, Y.; Solé-Benet, A.; Asensio, C.; Chamizo, S.; Puigdefábregas, J. Aggregate stability in range sandy loam soils relationships with runoff and erosion. *Catena* **2009**, *3*, 192–199. [CrossRef]
11. Vaezi, A.-R.; Ahmadi, M.; Cerdà, A. Contribution of raindrop impact to the change of soil physical properties and water erosion under semi-arid rainfalls. *Sci. Total Environ.* **2017**, *583*, 382–392. [CrossRef] [PubMed]
12. Yang, B.; Zhang, Y.-C.; Qian, Y.; Tang, J.; Liu, D.-Q. Climatic effects of irrigation over the Huang-Huai-Hai Plain in China simulated by the weather research and forecasting model. *J. Geophys. Res. Atmos.* **2016**, *5*, 2246–2264. [CrossRef]
13. Kang, S.; Eltahir, E.-A.-B. Impact of Irrigation on Regional Climate Over Eastern China. *Geophys. Res. Lett.* **2019**, *10*, 5499–5505. [CrossRef]
14. Liu, G.-S.; Wang, W.-G.; Shao, Q.-X.; Wei, J.; Zheng, J.-Z.; Liu, B.-J.; Chen, Z.-F. Simulating the Climatic Effects of Irrigation Over China by Using the WRF-Noah Model System With Mosaic Approach. *J. Geophys. Res. Atmos.* **2021**, *15*, e2020J–e34428J. [CrossRef]
15. Alewell, C.; Meusburger, K.; Brodbeck, M.; Bänninger, D. Methods to describe and predict soil erosion in mountain regions. *Landsc. Urban Plan.* **2008**, *2*, 46–53. [CrossRef]
16. Sun, W.-Y.; Shao, Q.-Q.; Liu, J.-Y.; Zhai, J. Assessing the effects of land use and topography on soil erosion on the Loess Plateau in China. *Catena* **2014**, *121*, 151–163. [CrossRef]
17. Jin, F.-M.; Yang, W.-C.; Fu, J.-X.; Li, Z. Effects of vegetation and climate on the changes of soil erosion in the Loess Plateau of China. *Sci. Total Environ.* **2021**, *773*, 145514. [CrossRef]
18. Yang, Z.-S.; Yang, L.; Wang, G.-L.; Hou, J.; Xin, Z.-B.; Liu, G.-H.; Fu, B.-J. The management of soil and water conservation in the Loess Plateau of China: Present situations, problems, and counter-solutions. *Acta Ecol. Sin.* **2019**, *20*, 7398–7409.

19. Wang, H.-J.; Yang, Z.-S.; Saito, Y.; Liu, J.-P.; Sun, X.-X.; Wang, Y. Stepwise decreases of the Huanghe (Yellow River) sediment load (1950–2005): Impacts of climate change and human activities. *Glob. Planet. Change* **2007**, *3–4*, 331–354. [CrossRef]
20. Zhao, X.-N.; Zhang, B.-Q.; Wu, P.-T. Changes in key driving forces of soil erosion in the Middle Yellow River Basin: Vegetation and climate. *Nat. Hazards* **2014**, *1*, 957–968. [CrossRef]
21. Wang, Y.-S.; Cheng, C.-C.; Xie, Y.; Liu, B.-Y.; Yin, S.-Q.; Liu, Y.-N.; Hao, Y.-F. Increasing trends in rainfall-runoff erosivity in the Source Region of the Three Rivers, 1961–2012. *Sci. Total Environ.* **2017**, *592*, 639–648. [CrossRef] [PubMed]
22. Tuo, D.-F.; Xu, M.-X.; Gao, G.-Y. Relative contributions of wind and water erosion to total soil loss and its effect on soil properties in sloping croplands of the Chinese Loess Plateau. *Sci. Total Environ.* **2018**, *633*, 1032–1040. [CrossRef] [PubMed]
23. Zhang, H.-W. Discussion on Development and Utilization of Water in Tibet. *Water Resour. Plan. Des.* **2011**, *1*, 1–4. (In Chinese)
24. Deng, M.-J. "Three Water Lines" strategy: Its spatial patterns and effects on water resources allocation in northwest China. *Acta Geogr. Sin.* **2018**, *7*, 1189–1203.
25. Zeng, Y.-J.; Xie, Z.-H.; Zou, J. Hydrologic and Climatic Responses to Global Anthropogenic Groundwater Extraction. *J. Clim.* **2017**, *1*, 71–90. [CrossRef]
26. Zhao, Y.; Huang, Y.; Wang, H.-J.; Xiao, W.-H.; Wang, H. Study on regional climate effect under water diversion in Northwest China. *J. Hydraul. Eng.* **2022**, *3*, 270–283. (In Chinese)
27. Vaezi, A.-R.; Zarrinabadi, E.; Auerswald, K. Interaction of land use, slope gradient and rain sequence on runoff and soil loss from weakly aggregated semi-arid soils. *Soil Tillage Res.* **2017**, *172*, 22–31. [CrossRef]
28. Wischmeier, W.-H.; Smith, D.-D. *Predicting Rainfall Erosion Losses*; A Guide to Conservation Planning; U.S. Department of Agriculture: Washington, DC, USA, 1978.
29. Laflen, J.-M.; Lane, L.-J.; Foster, G.-R. WEPP: A new generation of erosion prediction technology. *J. Soil Water Conserv.* **1991**, *1*, 34–38.
30. Renard, K.-G.; Foster, G.-R.; Weesies, G.-A. *Predicting Rainfall Ersion Losses: A Guide to Conservation Planning with the Revised Universal Soil Loss Equation (RUSLE)*; U.S. Department of Agriculture: Washington, DC, USA, 1997.
31. Xu, L.-F.; Xu, X.-G.; Meng, X.-W. Risk assessment of soil erosion in different rainfall scenarios by RUSLE model coupled with Information Diffusion Model: A case study of Bohai Rim, China. *Catena* **2013**, *100*, 74–82. [CrossRef]
32. Qin, W.; Guo, Q.-K.; Cao, W.-H.; Yin, Z.; Yan, Q.-H.; Shan, Z.-J.; Zheng, F.-L. A new RUSLE slope length factor and its application to soil erosion assessment in a Loess Plateau watershed. *Soil Tillage Res.* **2018**, *182*, 10–24. [CrossRef]
33. Teng, H.-F.; Rossel, R.-A.-V.; Shi, Z.; Behrens, T.; Chappell, A.; Bui, E. Assimilating satellite imagery and visible–near infrared spectroscopy to model and map soil loss by water erosion in Australia. *Environ. Model. Softw.* **2016**, *77*, 156–167. [CrossRef]
34. Teng, H.-F.; Jie, H.-U.; Yue, Z.; Zhou, L.-Q.; Zhou, S. Modelling and mapping soil erosion potential in China. *J. Integr. Agric.* **2019**, *2*, 251–264. [CrossRef]
35. Liu, B.-Y.; Xie, Y.; Zhang, K.-L. *Soil Erosion Forecast Model*; Science and Technology of China Press: Beijing, China, 2001.
36. Jiang, Z.-S.; Zheng, F.; Li, W.-M. Prediction model of water erosion on hillslopes. *J. Sediment Res.* **2005**, *4*, 1–6.
37. Marsland, S.-J.; Haak, H.; Jungclaus, J.-H.; Latif, M.; Röske, F. The Max-Planck-Institute global ocean/sea ice model with orthogonal curvilinear coordinates. *Ocean Model.* **2003**, *2*, 91–127. [CrossRef]
38. van Vuuren, D.-P.; Edmonds, J.; Kainuma, M.; Riahi, K.; Thomson, A.; Hibbard, K.; Hurtt, G.-C.; Kram, T.; Krey, V.; Lamarque, J.-F.; et al. The representative concentration pathways: An overview. *Clim. Change* **2011**, *1–2*, 5–31. [CrossRef]
39. Zhang, D.; Gao, X. Climate change of the 21st century over China from the ensemble of RegCM4 simulations. *Chin. Sci. Bull.* **2020**, *23*, 2516–2526. [CrossRef]
40. Wu, J.; Gao, X.-J. A gridded daily observation dataset over China region and comparison with the other datasets. *Chin. J. Geophys.* **2013**, *4*, 1102–1111. (In Chinese)
41. Giorgi, F.; Coppola, E.; Solmon, F.; Mariotti, L.; Sylla, M.-B.; Bi, X.; Elguindi, N.; Diro, G.-T.; Nair, V.; Giuliani, G.; et al. RegCM4: Model description and preliminary tests over multiple CORDEX domains. *Clim. Res.* **2012**, *52*, 7–29. [CrossRef]
42. Gao, X.-J.; Shi, Y.; Han, Z.-Y.; Wang, M.-L.; Wu, J.; Zhang, D.-F.; Xu, Y.; Giorgi, F. Performance of RegCM4 over Major River Basins in China. *Adv. Atmos. Sci.* **2017**, *4*, 441–455. [CrossRef]
43. Zou, J.; Zhan, C.-S.; Xie, Z.-H.; Qin, P.-H.; Jiang, S.-S. Climatic impacts of the Middle Route of the South-to-North Water Transfer Project over the Haihe River basin in North China simulated by a regional climate model. *J. Geophys. Res. Atmos.* **2016**, *15*, 8983–8999. [CrossRef]
44. Ministry Of Water Resources, PRC. *Standards for Classification and Gradartion of Soil Erosion (SL190-2007)*; Water Power Press: Beijing, China, 2008. (In Chinese)
45. Zhang, W.-B.; Xie, Y.; Liu, B.-Y. Rainfall Erosivity Estimation Using Daily Rainfall Amounts. *Sci. Geogr. Sin.* **2002**, *6*, 705–711. (In Chinese)
46. Ma, X.; He, Y.-D.; Xu, J.-C.; van Noordwijk, M.; Lu, X.-X. Spatial and temporal variation in rainfall erosivity in a Himalayan watershed. *Catena* **2014**, *121*, 248–259. [CrossRef]
47. McCool, D.-K.; Foster, G.-R.; Mutchler, C.-K.; Meyer, L.-D. Revised slope length factor for the Universal Soil Loss Equation. *Trans. ASAE* **1989**, *5*, 1571–1576. [CrossRef]
48. Cai, C.-F.; Ding, S.-W.; Shi, Z.-H.; Huang, L.; Zhang, G.-Y. Study of Applying USLE and Geographical Information System IDRISI to Predict Soil Erosion in Small Watershed. *J. Soil Water Conserv.* **2000**, *02*, 19–24. (In Chinese)

49. Dai, Z.-H.; Feng, X.-B.; Zhang, C.; Shang, L.-H.; Qiu, G.-L. Assessment of mercury erosion by surface water in Wanshan mercury mining area. *Environ. Res.* **2013**, *125*, 2–11. [CrossRef]
50. Lu, Q.-S.; Xu, B.; Liang, F.-Y.; Gao, Z.-Q.; Ning, J.-C. Influences of the Grain-for-Green project on grain security in southern China. *Ecol. Indic.* **2013**, *34*, 616–622. [CrossRef]
51. Shi, D.-M.; Chen, Z.-F.; Jiang, G.-Y.; Jiang, D. Comparative study on estimation methods for soil erodibility K in purple hilly area. *J. Beijing For. Univ.* **2012**, *1*, 32–38. (In Chinese)
52. Li, H.-W.; Xu, E.-Q.; Zhang, H.-Q. Soil erosion regionalization in Ili River Valley. *Chin. J. Agric. Resour. Reg. Plan.* **2018**, *4*, 116–124.
53. Ni, J.-R.; Li, X.-X.; Borthwick, A.-G.-L. Soil erosion assessment based on minimum polygons in the Yellow River basin, China. *Geomorphology* **2008**, *3*, 233–252. [CrossRef]
54. Fu, B.-J.; Liu, Y.; Lü, Y.-H.; He, C.-S.; Zeng, Y.; Wu, B.-F. Assessing the soil erosion control service of ecosystems change in the Loess Plateau of China. *Ecol. Complex.* **2011**, *4*, 284–293. [CrossRef]
55. Haddadchi, A.; Olley, J.; Pietsch, T. Using LM-OSL of quartz to distinguish sediments derived from surface-soil and channel erosion. *Hydrol. Process.* **2016**, *4*, 637–647. [CrossRef]
56. Han, X.-X.; Xiao, J.; Wang, L.-Q.; Tian, S.-H.; Liang, T.; Liu, Y.-J. Identification of areas vulnerable to soil erosion and risk assessment of phosphorus transport in a typical watershed in the Loess Plateau. *Sci. Total Environ.* **2021**, *758*, 143661. [CrossRef] [PubMed]
57. Guo, Q.-C.; Zheng, Z.; Huang, L.-M.; Deng, A.-J. Regularity of sediment transport and sedimentation during floods in the lower Yellow River, China. *Int. J. Sediment Res.* **2020**, *1*, 97–104. [CrossRef]
58. Walling, D.-E.; Webb, B.-W. Erosion and sediment yield: A global overview. *IAHS Publ. Ser. Proc. Rep. Intern Assoc Hydrol. Sci.* **1996**, *236*, 3–20.
59. Tang, K.-L. *Soil and Water Conservation in China*; Chinese Science Press: Beijing, China, 2004. (In Chinese)
60. Wang, F.-Q.; Wang, L.-J.; Peng, B.; Guo, W. Effect of flow and sediment variation on the Yellow River Delta wetland area evolution. *South–North Water Transf. Water Sci. Technol.* **2016**, *2*, 1–5.
61. Zhu, G.; Tang, Z.; Shangguan, Z.; Peng, C.; Deng, L. Factors Affecting the Spatial and Temporal Variations in Soil Erodibility of China. *J. Geophys. Res. Earth Surf.* **2019**, *3*, 737–749. [CrossRef]
62. Jiang, Q.; Zhou, P.; Liao, C.; Liu, Y.; Liu, F. Spatial pattern of soil erodibility factor (K) as affected by ecological restoration in a typical degraded watershed of central China. *Sci. Total Environ.* **2020**, *749*, 141609. [CrossRef]
63. Beillouin, D.; Cardinael, R.; Berre, D.; Boyer, A.; Corbeels, M.; Fallot, A.; Feder, F.; Demenois, J. A global overview of studies about land management, land-use change, and climate change effects on soil organic carbon. *Glob. Change Biol.* **2022**, *4*, 1690–1702. [CrossRef]
64. Ji, P.; Yuan, X.; Jiao, Y. Future hydrological drought changes over the upper Yellow River basin: The role of climate change, land cover change and reservoir operation. *J. Hydrol.* **2023**, *617*, 129128. [CrossRef]
65. Jiang, W.; Niu, Z.; Wang, L.; Yao, R.; Gui, X.; Xiang, F.; Ji, Y. Impacts of Drought and Climatic Factors on Vegetation Dynamics in the Yellow River Basin and Yangtze River Basin, China. *Remote Sens.* **2022**, *4*, 930. [CrossRef]
66. Li, C.; Raj Kattel, G.; Zhang, J.; Shang, Y.; Gnyawali, K.-R.; Zhang, F.; Miao, L. Slightly enhanced drought in the Yellow River Basin under future warming scenarios. *Atmos. Res.* **2022**, *280*, 106423. [CrossRef]
67. Omer, A.; Zhuguo, M.; Zheng, Z.; Saleem, F. Natural and anthropogenic influences on the recent droughts in Yellow River Basin, China. *Sci. Total Environ.* **2020**, *704*, 135428. [CrossRef] [PubMed]
68. Zhu, X.; Lee, S.; Wen, X.; Ji, Z.; Lin, L.; Wei, Z.; Zheng, Z.; Xu, D.; Dong, W. Extreme climate changes over three major river basins in China as seen in CMIP5 and CMIP6. *Clim. Dyn.* **2021**, *3*, 1187–1205. [CrossRef]
69. Bryan, B.-A.; Gao, L.; Ye, Y.; Sun, X.; Connor, J.-D.; Crossman, N.-D.; Stafford-Smith, M.; Wu, J.; He, C.; Yu, D.; et al. China's response to a national land-system sustainability emergency. *Nature* **2018**, *7713*, 193–204. [CrossRef] [PubMed]
70. Zhang, X.; She, D.; Cao, T.; Yang, Z.; He, C. Quantitatively identify the factors driving loess erodibility variations after ecological restoration. *Land Degrad. Dev.* **2022**, 1–14. [CrossRef]
71. Gao, X.-J.; Shi, Y.; Song, R.; Giorgi, F.; Wang, Y.; Zhang, D.-F. Reduction of future monsoon precipitation over China: Comparison between a high resolution RCM simulation and the driving GCM. *Meteorol. Atmos. Phys.* **2008**, *1–4*, 73–86. (In Chinese) [CrossRef]
72. Zhao, H.-F.; Lin, Y.-H.; Delang, C.-O.; Ma, Y.; Zhou, J.; He, H.-M. Contribution of soil erosion to the evolution of the plateau-plain-delta system in the Yellow River basin over the past 10,000 years. *Palaeogeogr. Palaeoclimatol. Palaeoecol.* **2022**, *601*, 111133. [CrossRef]
73. Knutti, R.; Sedláček, J. Robustness and uncertainties in the new CMIP5 climate model projections. *Nat. Clim. Chang.* **2013**, *4*, 369–373. [CrossRef]
74. Panagos, P.; Ballabio, C.; Himics, M.; Scarpa, S.; Matthews, F.; Bogonos, M.; Poesen, J.; Borrelli, P. Projections of soil loss by water erosion in Europe Byenvironmental Sci. *Policy* **2021**, *124*, 380–392.